

Karagozian & Case

2550 North Hollywood Way, Suite 500

Burbank, CA 91505-5026

www.kcse.com

EXPERIMENTAL RESULTS OF THE AISC FULL-SCALE COLUMN BLAST TEST

Joseph M. Magallanes
Ruben Martinez
John W. Koenig

March 21, 2006

Prepared for:

The American Institute of Steel Construction
1 East Wacker Drive., Suite 700
Chicago, IL 60601

Contract No. KC-05-27.2

EXPERIMENTAL RESULTS OF THE AISC FULL-SCALE COLUMN BLAST TEST

Joseph M. Magallanes
Ruben M. Martinez
John W. Koenig

March 21, 2006

Prepared for:

The American Institute of Steel Construction
1 East Wacker Drive., Suite 700
Chicago, IL 60601

Contract No. KC-05-27.2

EXECUTIVE SUMMARY

This summary report describes the full-scale blast test of a steel wide-flange column conducted for the American Institute of Steel Construction (AISC). Karagozian & Case (K&C) was the prime contractor and was responsible for creating the overall test plan, the design of the test article, the design of the reaction structure, and field coordination during the assembly and installation of the test article. The test was conducted by the Energetic Materials Research and Testing Center (EMRTC), subcontractor to K&C, on 02 March 2006 at the Multi-Bay Test Facility (MBTF) located within the EMRTC Field Laboratory in Socorro, NM.

The AISC column test investigated the behavior of a W14×233 column of ASTM A992, Gr. 50 structural steel, subjected to a large explosive, similar to that which can be expected in a terrorist attack on the exterior of a building with a vehicle bomb. The explosive, consisting of 4,000 pounds TNT-equivalent of Ammonium Nitrate/Fuel Oil (ANFO), was placed at a slant angle with respect to the column at an effective standoff of 15'-6" from the center of the column. The complete details of the column test specimen, reaction structure, explosive charge, and test results are summarized in this report.

ACKNOWLEDGEMENTS

Funding for the test was solely provided by AISC, with Mr. Charlie Carter serving as the project director. Mr. Carter's support, input, and guidance was extremely valuable to the entire effort, from planning the design of the test, to the review of the draft report. Substantial additional support was provided in the form of donation of time, services, and materials from numerous fabricators and engineers. K&C would specifically like to acknowledge the efforts of Mr. Tom Schlafly of AISC who coordinated the fabrication of the test article, Mr. Hans Warkentin from Trevian Projects Ltd. who donated numerous hours during Christmas of 2005 to generate the shop drawings of the test article, and Mr. Bill Lindley of the W&W Steel Co. who generously donated and fabricated all steel materials for the test article. Finally, the input and suggestions of various engineers were extremely valuable to this project. In particular Dr. Jack Hayes of the National Institute of Science and Technology, Dr. Stanley Woodson of the Engineering Research and Development Center, Construction Engineering Research Laboratory, and Mr. David Bonneville and Mr. Robert Pekelnicky of Degenkolb Engineers.

TABLE OF CONTENTS

Section	Page
EXECUTIVE SUMMARY	i
ACKNOWLEDGEMENTS	ii
FIGURES	iii
TABLES	v
1 INTRODUCTION	1-1
1.1 SCOPE	1-1
1.2 TEST BACKGROUND	1-1
1.3 TEST OBJECTIVE	1-2
1.4 ORGANIZATION OF THE REPORT	1-2
2 TEST BED SETUP	2-1
2.1 TEST ARTICLE	2-1
2.2 INSTALLATION TO THE REACTION STRUCTURE	2-1
2.3 INSTALLATION OF CLADDING	2-2
2.4 CHARGE AND STANDOFF	2-3
2.5 INSTRUMENTATION AND HIGH-SPEED VIDEO	2-4
2.6 PRETEST PREDICTION	2-4
3 TEST RESULTS	3-1
3.1 OBSERVED RESULTS	3-1
3.2 COLUMN RESIDUAL DEFLECTION	3-2
4 DISCUSSION OF RESULTS	4-1
4.1 RESPONSE OF COLUMN	4-1
4.2 STEEL FRACTURE	4-2
5 CONCLUSIONS	5-1
5.1 CONCLUSIONS	5-1
5.2 RECOMMENDATIONS	5-1
6 REFERENCES	6-1
Appendix	
A TEST SPECIMEN CONSTRUCTION DOCUMENTS	A-1

FIGURES

Figure		Page
1-1	Explosive threat of interest to the FEMA/DHS study	1-3
1-2	The FEMA/DHS study focused on the 14WF228 column at gridlines G3 subjected to a 4,000-pound TNT equivalent explosive	1-4
1-3	Section properties of the 14WF228 column	1-5
2-1	The AISC test column specimen.....	2-6
2-2	Section properties of the W14×233 column	2-7
2-3	Photograph of the column base and header assemblies prior to filling with concrete	2-8
2-4	Reaction wall at the MBTF site at EMRTC.....	2-9
2-5	Photographs of the installation of the test article to the MBTF reaction wall	2-10
2-6	Photographs of the of the test article during curing of the footing	2-11
2-7	Installation of the brick cladding enclosure around the test column	2-12
2-8	Chronological view of AISC steel column cladding installation.....	2-13
2-9	Photograph of the completed test column including the cladding enclosure.....	2-14
2-10	Illustration of the positioning of the explosive to achieve an effective slant standoff of 15'-6" measured from the center of the column to the center of the charge.....	2-15
2-11	Photograph of a similar ANFO explosive setup using a Sonotube.....	2-16
2-12	Pretest photographs of the charge stand and explosive positioned at an effective slant standoff of 15'-6" measured from the center of the column to the center of the charge in the direction normal to the MBTF reaction wall.....	2-17
2-13	Estimate of the air blast loadings from 4,000 lb TNT at 15' standoff	2-18
2-14	Air blast loadings versus range for an ideal 4,000-pound TNT hemisphere on the ground surface.....	2-18
2-15	High-speed video camera details	2-19
3-1	Close-up video stills of the test bed moments after detonation	3-4
3-2	Video stills of the test bed moments after detonation.....	3-6
3-3	Posttest photograph of the crater left by the explosion.....	3-8
3-4	Pre and posttest photographs of the column	3-9
3-5	Posttest photographs of the column and reaction system	3-10
3-6	Close-up posttest photograph of the column	3-11

FIGURES (CONTINUED)

Figure		Page
3-7	Posttest photographs of the base of the column.....	3-13
3-8	Process of conducting the posttest survey of the column to quantify the residual deflection of the column's front flange as a function of height along the column	3-14
3-9	Residual deflection of the column's front flange as a function of height along the column.....	3-15
4-1	Variations in the response of steel wide-flange columns with and without cladding...	4-3
4-2	Response of the 14WF228 column as computed simplified HFPB FE calculations for the FEMA/GSA effort that included simplify loading methodologies	4-5
4-3	Failure modes of wide-flange sections as observed in a separate test program funded by AISC	4-6

TABLES

Table	Page
2-1 High-speed video camera information.....	2-5
3-1 Residual deflection of the column as measured in a posttest survey	3-3

SECTION 1

INTRODUCTION

1.1 SCOPE

This summary report describes the full-scale blast test of a steel wide-flange column conducted for, and funded by, the American Institute of Steel Construction (AISC). Karagozian & Case (K&C) was the prime contractor and was responsible for creating the overall test plan, the design of the test article, the design of the reaction structure, and field coordination during the assembly and installation of the test article. The test was conducted by the Energetic Materials Research and Testing Center (EMRTC), subcontractor to K&C, on 02 March 2006 at the Multi-Bay Test Facility (MBTF) located within the EMRTC Field Laboratory in Socorro, NM.

The AISC column test investigated the behavior of a W14x233 column of ASTM A992, Gr. 50 structural steel, subjected to a large explosive, similar to that which can be expected in a terrorist attack on the exterior of a building with a vehicle bomb. The explosive, consisting of 4,000 pounds TNT equivalent of Ammonium Nitrate/Fuel Oil (ANFO), was placed at a slant angle with respect to the column at an effective standoff of 15'-6" from the center of the column. The complete details of the column test specimen, reaction structure, explosive charge, and test results are summarized in this report.

1.2 TEST BACKGROUND

The Federal Emergency Management Agency (FEMA) and the Department of Homeland Security (DHS) have recently joined efforts in conducting a study on steel structures regarding the blast-resistant benefits gained by implementing current seismic design and detailing requirements. This effort is similar to a previous study focusing on reinforced concrete buildings [1]. The current FEMA/DHS effort is being executed with a joint effort between the U.S. Army Corps of Engineers Engineering Research and Development Center (ERDC), out of Vicksburg, MS, and Degenkolb Engineers, based out of San Francisco, CA. Numerous experts in various disciplines encompassing the study, such as steel fracture, blast effects, and seismic design, serve on a peer review panel for this FEMA/DHS study and include members of AISC and K&C.

The study focused on a modified version of an existing steel structure subjected to an explosive charge similar to that experienced during the terrorist attack on the Murrah Building in Oklahoma City in 1995. The scenario of interest to the study is illustrated in Figure 1-1. The structure consists of a steel-framed gravity system supporting a steel metal deck with concrete infill and relies on moment-frames as the building's primary lateral force-resisting system (LFRS). Since the structure reflects older LFRS detailing requirements, several building retrofits were considered to upgrade the existing building to conform to current seismic design requirements for areas of high seismicity (e.g., San Francisco, CA). A blast effects analysis of each retrofit scheme was executed to quantify the blast resistant benefits obtained through implementing these various seismic upgrade schemes.

A threat representative of the attack on the Murrah Building was determined by the FEMA/DHS peer review panel to be a 4,000-pound TNT-equivalent charge positioned away from the column at gridline G3 as illustrated in Figure 1-2. This equated to an effective slant standoff of 15'-6" from the center of this column to the center of the explosive source.

The column at gridline G3 is an older AISC 14WF228 section [2]. As summarized in Figure 1-3, the column has a section depth of 16 inches with a nominal web thickness of 1.045 inches, and nominal flange width and thickness of 15.865 and 1.688 inches, respectively. In the FEMA/DHS structure, the column was founded in a concrete pilaster within a 10 inch thick concrete retaining wall as was shown in Figure 1-2. The column was continuous through the second floor and framed by three W24× girders on three sides, each having moment connections to the column. The column also had a 2'-6" square architectural enclosure composed of 2-inch thick marble cladding. The clear height from the top of the base concrete to the bottom of the W24× girder is 18'-9".

The study, near its completion at the time of the delivery of this report, will conclude important findings that will be available for reference by both the construction and engineering design communities. However, one source of uncertainty at this moment is the actual behavior of the first story column at gridline G3. If the column is significantly damaged from the explosion, the result may be a situation in which large redistribution demands are created on the exterior perimeter frames in the evaluation of progressive collapse potential. Determining the behavior of this column is paramount to the conclusions drawn from this FEMA/DHS study.

1.3 TEST OBJECTIVE

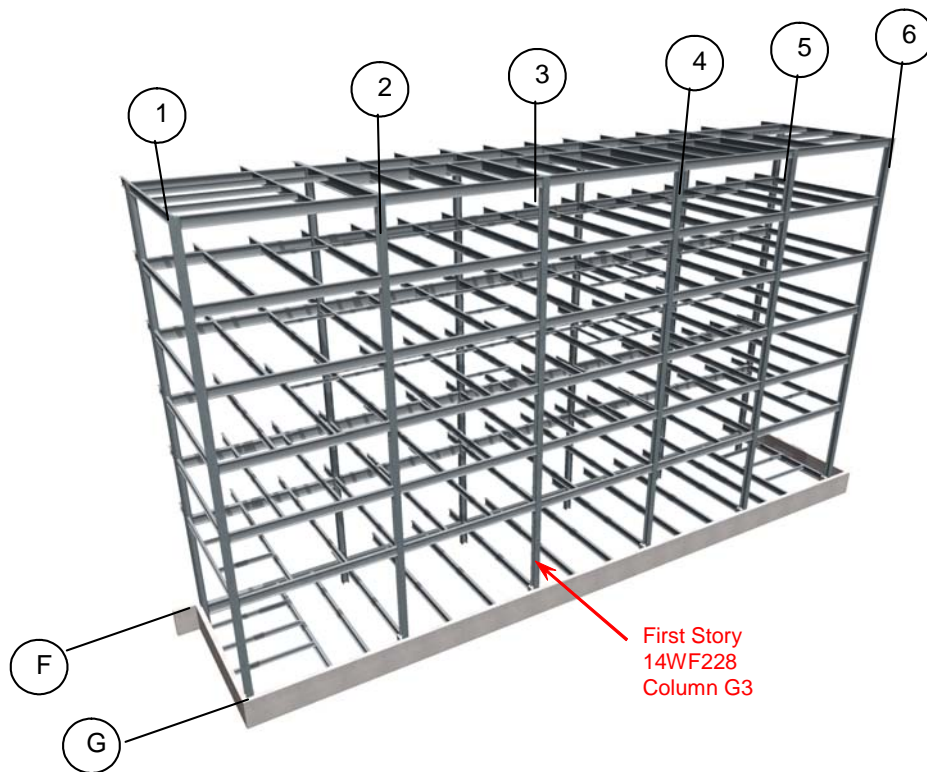
Spurred by this FEMA/DHS effort, the American Institute of Steel Construction (AISC) contracted K&C, with EMRTC as its subcontractor, to execute a blast test of a representative test article of this steel column. Hence, the primary objective of this test was to experimentally determine the response of the column subjected to a 4000-pound TNT-equivalent explosion at an effective slant range of 15'-6".

1.4 ORGANIZATION OF THE REPORT

This report is divided up into several sections to provide a concise summary of the test conducted to achieve this objective. Section 2 describes the test bed setup. Included in this discussion is a detailed summary of the test article, supporting structure, explosive, and the active instrumentation fielded for the test. Section 3 contains the test results. Here, high-speed video photography of the test is shown and the response of the column illustrated with posttest photographs. Section 4 provides a discussion of the test results. Section 5 summarizes the important conclusions gained from the test and provides recommendations for future research.



(a) Attack scenario of interest.



(b) Steel framing.

Figure 1-1. Explosive threat of interest to the FEMA/DHS study.

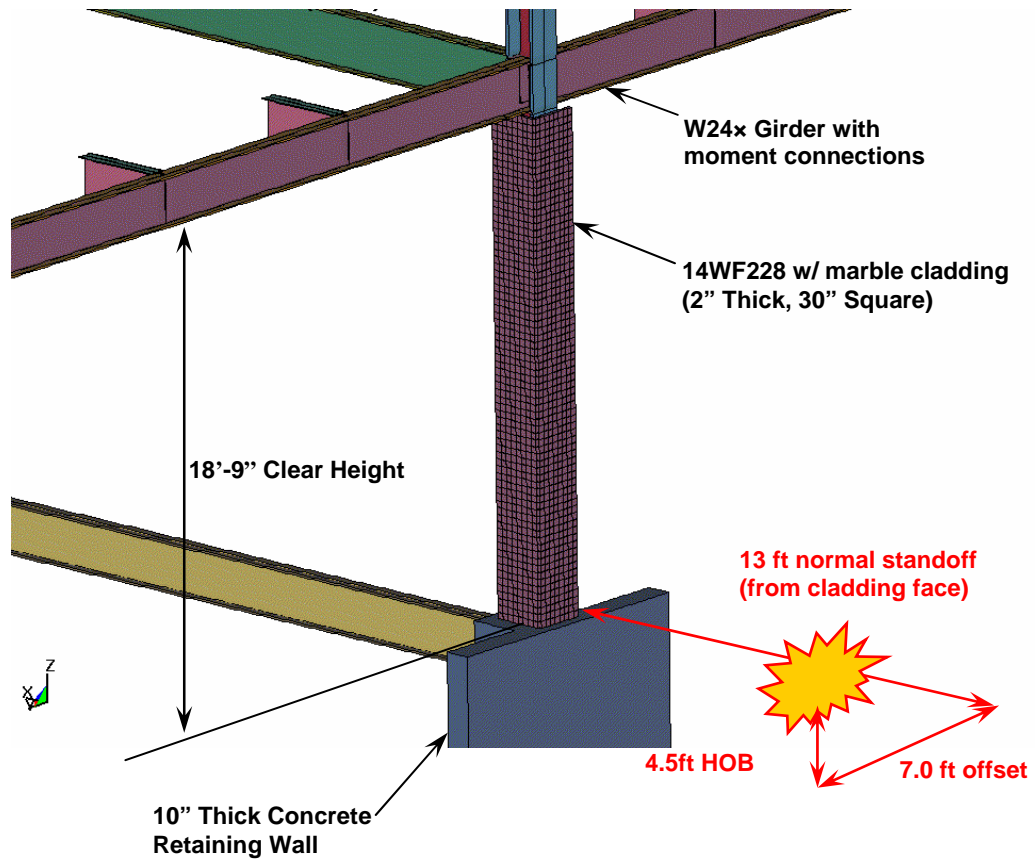


Figure 1-2. The FEMA/DHS study focused on the 14WF228 column at gridlines G3 subjected to a 4,000-pound TNT equivalent explosive.

14" COLUMNS																		
REFERENCES; SEE COLUMN (I) AND PAGE 4																		
SECT. NO. OR NOM. SIZE	COL (1)	WEIGHT		DEPTH d in.	FLANGE		WEB THICK t in.	DIMENSIONS				SLOPE INSIDE FLANGE %	AXIS 1-1			AXIS 2-2		
		PER FOOT	AREA		WIDTH b in.	m		n	R	R'	I		S	r	I	S	r	
		Lb.	Sq.in.		in.	in.		in.	in.	in.	in.		in. ⁴	in. ⁴	in.	in. ⁴	in. ⁴	in.
H14b 1		265.1	77.97	16.500	15.040	1.290	2.130	1.992	.60	0	2.0	3457.0	419.0	6.66	1153.3	153.4	3.85	
CB146 10 14X15		265.0	77.93	16.332	15.826	1.232	1.971	1.971	.65	0	0	3442.4	421.6	6.65	1304.2	164.8	4.09	
14WF 14X16 7.8,9,13,15		264.0	77.63	16.500	16.025	1.205	1.938	1.938	.60	0	0	3526.0	427.4	6.74	1331.2	166.1	4.14	
CB146N 12 14X16		264.0	77.62	16.500	16.026	1.206	1.938	1.938	.65	0	0	3525.4	427.3	6.74	1331.5	166.2	4.14	
H14 4		262.5	76.93	16.500	14.780	1.290	2.130	1.995	.60	0	2.0	3402.1	412.4	6.65	1095.6	148.3	3.77	
H14 5		262.0	77.20	16.375	15.450	1.230	2.067	1.925	.60	0	2.0	3413.4	416.9	6.65	1209.0	156.5	3.96	
H14 2		261.5	76.93	16.500	14.780	1.290	2.130	1.995	.60	0	2.0	3402.1	412.4	6.65	1095.6	148.3	3.77	
H14b 1		256.5	75.43	16.380	15.000	1.250	2.067	1.930	.60	0	2.0	3315.4	404.9	6.63	1108.7	147.8	3.83	
CB146 10 14X15		255.0	74.99	16.192	15.781	1.187	1.901	1.901	.65	0	0	3280.0	405.1	6.61	1247.1	158.0	4.08	
CB146N 12 14X16		255.0	74.98	16.370	15.992	1.172	1.873	1.873	.65	0	0	3372.3	412.0	6.71	1278.6	159.9	4.13	
14WF 14X16 7.8,13,15		255.0	74.98	16.370	15.990	1.170	1.873	1.873	.60	0	0	3372.6	412.0	6.71	1278.1	159.9	4.13	
H14 5		254.0	74.62	16.250	15.410	1.190	2.005	1.862	.60	0	2.0	3270.6	402.5	6.62	1161.2	150.7	3.94	
H14 4		254.0	74.43	16.380	14.740	1.250	2.067	1.933	.60	0	2.0	3262.7	398.5	6.62	1053.2	142.9	3.76	
H14 2		253.0	74.43	16.380	14.740	1.250	2.067	1.933	.60	0	2.0	3262.7	398.5	6.62	1053.2	142.9	3.76	
H14b 1		247.9	72.91	16.250	14.960	1.210	2.005	1.867	.60	0	2.0	3176.3	390.9	6.60	1064.7	142.3	3.82	
CB146N 12 14X16		246.0	72.33	16.250	15.947	1.127	1.813	1.813	.65	0	0	3228.6	397.4	6.68	1227.1	153.9	4.12	
14WF 14X16 7.8,9,13,15		246.0	72.33	16.250	15.945	1.125	1.813	1.813	.60	0	0	3228.9	397.4	6.68	1226.6	153.9	4.12	
H14 4		245.5	71.94	16.250	14.700	1.210	2.005	1.870	.60	0	2.0	3125.8	384.7	6.59	1011.3	137.6	3.5	
CB146 10 14X15		245.0	72.06	16.050	15.738	1.144	1.830	1.830	.65	0	0	3119.6	388.7	6.58	1190.6	151.3	4.06	
H14 5		245.0	72.05	16.125	15.370	1.150	1.942	1.800	.60	0	2.0	3130.4	388.3	6.59	1114.2	145.0	3.93	
H14 2		244.5	71.94	16.250	14.700	1.210	2.005	1.870	.60	0	2.0	3125.8	384.7	6.59	1011.3	137.6	3.75	
H14b 1		239.3	70.39	16.130	14.920	1.170	1.942	1.805	.60	0	2.0	3039.9	377.0	6.57	1021.4	136.9	3.81	
14WF 14X16 7.8,9,13,15		237.0	69.69	16.120	15.910	1.090	1.748	1.748	.60	0	0	3080.9	382.2	6.65	1174.8	147.7	4.11	
CB146N 12 14X16		237.0	69.68	16.120	15.911	1.091	1.748	1.748	.65	0	0	3080.2	382.2	6.65	1175.0	147.7	4.11	
H14 4		237.0	69.45	16.130	14.660	1.170	1.942	1.808	.60	0	2.0	2991.5	371.0	6.56	970.0	132.3	3.74	
H14 5		236.0	69.49	16.000	15.330	1.110	1.880	1.737	.60	0	2.0	2992.9	374.1	6.56	1067.8	139.3	3.92	
H14 2		236.0	69.45	16.130	14.660	1.170	1.942	1.808	.60	0	2.0	2991.5	371.0	6.56	970.0	132.3	3.74	
CB146 10 14X15		235.0	69.11	15.908	15.693	1.099	1.759	1.759	.65	0	0	2961.9	372.4	6.55	1134.5	144.6	4.05	
H14b 1		230.8	67.89	16.000	14.880	1.130	1.880	1.742	.60	0	2.0	2905.9	363.2	6.55	978.7	131.5	3.80	
H14 4		228.5	66.98	16.000	14.620	1.130	1.880	1.745	.60	0	2.0	2859.6	357.5	6.53	929.4	127.1	3.72	
14WF 14X16 7.8,9,13,14		228.0	67.06	16.000	15.865	1.045	1.688	1.688	.60	0	0	2942.4	367.8	6.62	1124.8	141.8	4.10	
CB146N 12 14X16		228.0	67.03	16.000	15.865	1.045	1.688	1.688	.65	0	0	2941.4	367.7	6.62	1124.7	141.8	4.10	

Figure 1-3. Section properties of the 14WF228 column [2].

This Page is Intentionally Left Blank

SECTION 2

TEST BED SETUP

2.1 TEST ARTICLE

A test article was designed to replicate the most critical geometric and structural features of the FEMA/DHS column which would affect the behavior of the column in a blast environment. Such features included the column materials, steel section shape, boundary conditions, and the service column axial loads. Capturing all features was found to be too costly and unnecessary altogether, considering the overall objectives of the test. Hence, given the resources and funding available, all of these features were included with the exception of the axial load. However, given the rather large cross section and the relatively light axial loads in the actual column, the exclusion of this effect was not expected to significantly alter the overall response of the column.

A test article was designed and structural drawings issued for construction. These are shown in Appendix A, including the shop drawings upon which the specimen was fabricated. A structural elevation of the test article, reproduced from Appendix A, is shown in Figure 2-1a. A photograph of the test article upon delivery to EMRTC is shown in Figure 2-1b.

The test column was an AISC W14x233 standard rolled shape of ASTM A992, Gr.50 structural steel, as this section possesses the most similar cross-section properties to the 14WF228 section used in the FEMA/DHS column study. The cross-section properties of the W14x233 column is shown in Figure 2-2 [3]. The test article had a clear span of 18'-9" measured from the top of the reinforced concrete (RC) base assembly to the bottom of the RC header assembly. Both the base and header reaction assemblies were constructed of a series of ¼" thick steel plates shaped into a box which had the dual purpose of serving as a perimeter where the steel struts could be welded, in addition to serving as forms for the concrete pour. Nelson studs welded to the sides of each steel plate facilitated this connection to the concrete. At each end of the column, these base and header assemblies were connected to the column via full-penetration welds. Photographs of the base and header reaction assemblies are shown in Figure 2-3, prior to filling each with concrete. When filled with concrete, the base and header assemblies provided fixed boundary constraints at each end of the column.

2.2 INSTALLATION TO THE REACTION STRUCTURE

The column specimen was installed at the Multi-Bay Test Facility (MBTF) located within the EMRTC Field Laboratory in Socorro, NM. The reaction wall at the MBTF site is a large and massive structure capable of developing large reactive loads and was designed for the high explosive (HE) testing of components placed at short distances to the front of its armor steel plate wall. For the AISC column test, the structure was modified to accommodate the column specimen and associated connection hardware for the header, base, the RC slab, and the eight header reaction struts. Two photographs of the MBTF reaction wall are shown in Figure 2-4; the

first taken before the modifications and the second after the modification but before the installation of the test specimen. These modifications included:

- removal of the existing platform, support bracing and other unnecessary components;
- earth-moving work to form a uniform, horizontal surface between the charge location and test specimen as well as for adequate in-fill behind the reaction wall;
- placement of the 2-ft thick trapezoidal shaped reinforced concrete slab beginning 3 ft before the structure; and
- preparation and installation of the bolted steel channels to the armor steel plate wall for the upper strut reaction system.

The column was erected at the MBTF site on 03 February 2006. As shown in Figure 2-5, the column's top-most rear reaction struts were connected to the reaction wall to stabilize the column while the concrete base and trapezoidal slab on grade poured with concrete. Figure 2-6 shows the column during the curing of the footing.

2.3 INSTALLATION OF CLADDING

Several different material options were explored for use as a surrogate cladding around the column test specimen. Obviously, installation of the marble cladding identical to that of the original structure was not feasible. The major discriminator for the substitute material was that its mass should be relatively close to that of the marble it replaced. After researching various materials (including pre-cast hollow-core concrete panels, cast-in-place concrete panels, granite panels), AISC and K&C chose to use modular clay face brick.

The red clay bricks used for the test have a density of 100 pcf which equates to roughly 30 psf for the 3-5/8" deep brick at the column. The marble in the FEMA/DHS structure was 2" thick, and was installed with a clear spacing of 3 inches, from all column edges. Marble density can vary greatly, but can be up to 200 pcf which equates to 33 pcf for the 2-inch thick material used at the FEMA/DHS column. Thus, the clay face-brick provided a readily available and low cost material substitute that was very close in density to the marble of the original structure.

Construction on the cladding began during the curing of the concrete at the base. A photograph after the first lift is shown in Figure 2-7. Grout was not used to fill the voids in the brick, thus the brick density was not increased. Each face of the cladding enclosure was attached to the column with steel corrugated wall ties that were tack welded to the column at each lift—a detail used in the FEMA/DHS building. This connection was provided to supply lateral stability to the cladding as is commonly done in practice.

Figure 2-8 are chronological stills that show the progress of the cladding installation. A photograph of the completed test column, including both the cladding and the completed reaction strut assembly, is shown in Figure 2-9.

2.4 CHARGE SIZE AND STANDOFF

The explosive used for the column test was 4,860 pounds of ANFO, which approximately equates to 4,000 pounds of equivalent-TNT. During the design of the test article, the column was oriented roughly 27 degrees from a normal directed outward away from the MBTF reaction wall. This is shown in Figure 2-10. This was done so that the charge, the header reaction assembly, and the strut reaction system would remain perfectly normal to the wall, thus minimizing eccentric loading into the upper reaction system. For this reason, the charge was placed 167 inches from the center of the column in a direction normal to the strong axis of the column with an 87-inch offset to achieve the 188-inch (15'-6") effective slant standoff to the center of the charge, as shown in Figure 2-10a.

The explosive was poured into a 5-foot diameter container, to create an ideal cylindrically-shaped charge, up to a height slightly over 4'-10", as shown in Figure 2-10b. Hence, the aspect ratio of the charge was approximately 1 to 1. The charge was placed atop a wooden stand sitting directly on grade, which corresponded with the top surface of the column footer. The charge stand was constructed with 2"x4" bracing, 4"x4" legs, and a 3/4 inch plywood top, to achieve the desired height of burst (HOB) of 4'-6".

On the day of the test, the charge stand was positioned as described in the preceding paragraphs. The charge was built by first placing half of the ANFO into the container. A 15-pound C-4 booster charge that featured two RP 83 detonators, wired in series, was then placed on the surface of the ANFO at its center. Next, an RG 58 detonation cable was spliced to the detonator wires and routed across the surface of the ANFO and up one side of the Sonotube, attaching it to the inside surface with tape. The remainder of the ANFO was then added to the Sonotube to complete the charge for the test. A similar setup is shown in Figure 2-11. Two views of the completed test bed are shown in Figure 2-12.

Anticipated airblast loads were computed with the fast-running computer program ConWep [4]. ConWep is a program that uses the Kingery-Bulmash curves found in TM 1300 [5] and TM 5-855-1 [6], which are equations for airblast loadings based on explosive tests using charge weights from less than 1 kg to over 400,000 kg. As no pressure sensors were fielded for this test, these predictions are provided for reference purposes, only. These loads will only provide an estimate of the actual loads, since the charge is placed at a very short scaled range from the test article (less than 1.0 in this case), and the shape of the explosive and its detonation mechanism will have a clear effect on the loading distribution. Only a detailed hydrocode calculation using computational fluid dynamics (CFD) is capable of predicting this loading with reasonable accuracy. Due to budgetary constraints, this type of calculation was not performed. Instead, an ideal hemisphere of explosive situated on the ground is assumed, whereas, the actual charge is an elevated cylinder 4.5 feet above the ground surface. Figure 2-13a presents the reflected pressure and impulse history loadings for a 4,000-pound TNT equivalent charge at a standoff of 15 feet given these simplifications. Similarly, Figure 2-13b presents the incident pressure and impulse history loading for the same charge and standoff. Figure 2-14 is a more generalized plot that shows the reflected and incident pressures and impulses as a function of standoff for the 4,000-pound charge. The complete output text file from the ConWep program, which lists several other airblast loading parameters, is listed in Figure A-5 of Appendix A.

2.5 INSTRUMENTATION AND HIGH-SPEED PHOTOGRAPHY

Due to program funding limitations, the column test specimen was not instrumented with any active channels for accelerometers, linear variable-displacement transducers (LVDT), or pressure gages. However, three high-speed digital cameras (Phantom v7.0 Series by Vision Research, Inc.) were employed to record both close-in and overall test bed views of the explosive event. These cameras are capable of capturing high-quality video at frame rates exceeding 100,000 frames per second. Typical frame rates used for coverage of past structural response tests range from 1,000 – 4,000 frames per second.

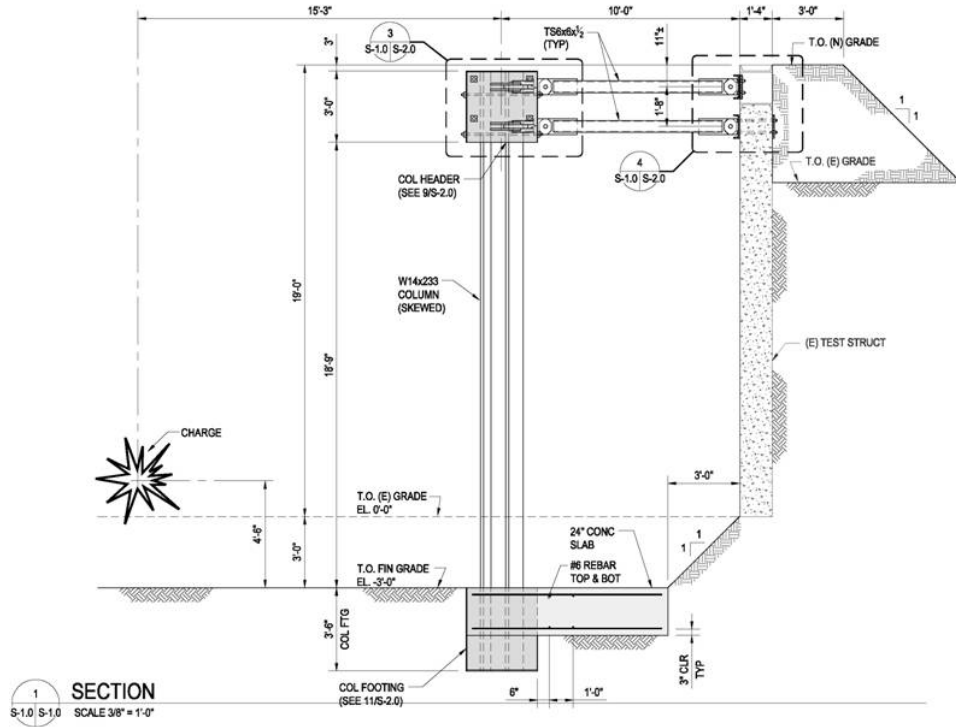
The closest camera was placed a short distance to the east and above the charge by several tens of feet. This camera, PC-1, was fielded in order to provide a clear, unobstructed view of the fireball and shock front as they approached the test specimen and reaction wall. The second camera, PC-2, was placed at a slightly greater distance from the charge as the first camera, but to the northeast and at an elevation that closely matched that of the charge. The third camera, PC-3, was similarly placed in a north-northeast position relative to the charge, also at an elevation that matched that of the charge. These last two cameras provided more of an overview of the event, as the initial flash and ensuing fireball quickly obscure the test bed. Table 2-1 provides additional information with regards to these Phantom cameras. Figure 2-14b shows a photograph viewing from atop the MBTF Reaction Wall in which the locations of the three Phantom cameras are identified. Also identified in this figure is a north key referenced in the following sections, which indicates north normal to the reaction wall.

2.6 PRETEST PREDICITONS

Due to budgetary constraints, a pretest prediction using high-fidelity physics-based (HFPB) finite element (FE) models and computational solid dynamics (CSD) was not performed for the response of the test article. K&C typically performed HFPB CFD and CSD computations on test articles to estimate the behaviors and make changes to the test to optimize the most useful test bed arrangements given the objectives of the test. Although a detailed calculation of this type was not performed, a much more simplified calculation was conducted for the FEMA/DHS effort that provides an estimate of the column response [7]. This calculation is discussed later in Section 4.

Table 2-1. High-speed video camera information.

Camera	Video Filename	Location From Charge	Frame Rate (fps)	Interval (μs)	Exposure (μs)	Report Figures
PC-1	TEST 1 CLOSEUP.cin	E	4801.921	208.25	6	3-4
PC-2	TEST 1 MEDIUM VIEW.cin	NE	4801.921	208.25	10	—
PC-3	TEST 1.cin	N-NE	300.008	3333.25	20	3-5



(a) Structural detail of the test article.



(b) Fabricated column specimen prior to installation.

Figure 2-1. The AISC test column specimen.

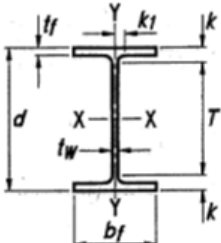


**Table 1-1 (cont.)
W-Shapes
Dimensions**

Shape	Area, A	Depth, d		Web			Flange			Distance					
				Thickness, t _w	t _w /2	Width, b _f	Thickness, t _f	k		T	Work- able Gage†				
								in.	in.			in.	in.	in.	in.
in.²	in.	in.	in.	in.	in.	in.	in.	in.	in.	in.	in.	in.			
W18×71	20.8	18.5	18 1/2	0.495	1/2	1/4	7.64	7 5/8	0.810	13/16	1.21	1 1/2	7/8	15 1/2	3 1/2
×65	19.1	18.4	18 3/8	0.450	7/16	1/4	7.59	7 5/8	0.750	3/4	1.15	1 7/16	7/8	↓	↓
×60	17.6	18.2	18 1/4	0.415	7/16	1/4	7.56	7 1/2	0.695	11/16	1.10	1 3/8	13/16	↓	↓
×55	16.2	18.1	18 1/8	0.390	3/8	3/16	7.53	7 1/2	0.630	5/8	1.03	1 5/16	13/16	↓	↓
×50	14.7	18.0	18	0.355	3/8	3/16	7.50	7 1/2	0.570	9/16	0.972	1 1/4	13/16	↓	↓
W18×46	13.5	18.1	18	0.360	3/8	3/16	6.06	6	0.605	5/8	1.01	1 1/4	13/16	15 1/2	3 1/2
×40	11.8	17.9	17 7/8	0.315	5/16	3/16	6.02	6	0.525	1/2	0.927	1 3/16	13/16	↓	↓
×35	10.3	17.7	17 3/4	0.300	5/16	3/16	6.00	6	0.425	7/16	0.827	1 1/8	3/4	↓	↓
W16×100	29.7	17.0	17	0.585	9/16	5/16	10.4	10 3/8	0.985	1	1.69	1 7/8	1 1/8	13 1/4	5 1/2
×89	26.4	16.8	16 3/4	0.525	1/2	1/4	10.4	10 3/8	0.875	7/8	1.58	1 3/4	1 1/16	↓	↓
×77	22.9	16.5	16 1/2	0.455	7/16	1/4	10.3	10 1/4	0.760	3/4	1.47	1 5/8	1 1/16	↓	↓
×67	20.0	16.3	16 3/8	0.395	3/8	3/16	10.2	10 1/4	0.665	11/16	1.37	1 9/16	1	↓	↓
W16×57	16.8	16.4	16 3/8	0.430	7/16	1/4	7.12	7 1/8	0.715	11/16	1.12	1 3/8	7/8	13 5/8	3 1/2
×50	14.7	16.3	16 1/4	0.380	3/8	3/16	7.07	7 1/8	0.630	5/8	1.03	1 5/16	13/16	↓	↓
×45	13.3	16.1	16 1/8	0.345	3/8	3/16	7.04	7	0.565	9/16	0.967	1 1/4	13/16	↓	↓
×40	11.8	16.0	16	0.305	5/16	3/16	7.00	7	0.505	1/2	0.907	1 3/16	13/16	↓	↓
×36	10.6	15.9	15 7/8	0.295	5/16	3/16	6.99	7	0.430	7/16	0.832	1 1/8	3/4	↓	↓
W16×31	9.13	15.9	15 7/8	0.275	1/4	1/8	5.53	5 1/2	0.440	7/16	0.842	1 1/8	3/4	13 5/8	3 1/2
×26	7.68	15.7	15 3/4	0.250	1/4	1/8	5.50	5 1/2	0.345	3/8	0.747	1 1/16	3/4	13 5/8	3 1/2
W14×806*	237	22.8	22 7/8	3.74	3 3/4	1 7/8	18.6	18 1/2	5.12	5 1/8	5.72	6 7/16	3 1/16	10	3-7 1/2-3
×730*	215	22.4	22 3/8	3.07	3 1/16	1 9/16	17.9	17 7/8	4.91	4 15/16	5.51	6 3/16	2 3/4	↓	3-7 1/2-3
×665*	196	21.6	21 5/8	2.83	2 13/16	1 7/16	17.7	17 5/8	4.52	4 1/2	5.12	5 13/16	2 5/8	↓	↓
×605*	178	20.9	20 7/8	2.60	2 5/8	1 9/16	17.4	17 3/8	4.16	4 3/16	4.76	5 7/16	2 1/2	↓	↓
×550*	162	20.2	20 1/4	2.38	2 3/8	1 3/16	17.2	17 1/4	3.82	3 13/16	4.42	5 5/8	2 3/8	↓	↓
×500*	147	19.6	19 5/8	2.19	2 3/16	1 1/8	17.0	17	3.50	3 1/2	4.10	4 13/16	2 5/16	↓	↓
×455*	134	19.0	19	2.02	2	1	16.8	16 7/8	3.21	3 3/16	3.81	4 1/2	2 1/4	↓	↓
×426*	125	18.7	18 5/8	1.88	1 7/8	15/16	16.7	16 3/4	3.04	3 1/16	3.63	4 5/16	2 1/8	↓	↓
×398*	117	18.3	18 1/4	1.77	1 3/4	7/8	16.6	16 5/8	2.85	2 7/8	3.44	4 1/8	2 1/8	↓	↓
×370*	109	17.9	17 7/8	1.66	1 5/8	13/16	16.5	16 1/2	2.66	2 11/16	3.26	3 15/16	2 1/16	↓	↓
×342*	101	17.5	17 1/2	1.54	1 9/16	13/16	16.4	16 3/8	2.47	2 1/2	3.07	3 3/4	2	↓	↓
×311*	91.4	17.1	17 1/8	1.41	1 7/16	3/4	16.2	16 1/4	2.26	2 1/4	2.86	3 9/16	1 15/16	↓	↓
×283*	83.3	16.7	16 3/4	1.29	1 5/16	11/16	16.1	16 1/4	2.07	2 1/16	2.67	3 3/8	1 7/8	↓	↓
×257*	75.6	16.4	16 3/8	1.18	1 3/16	5/8	16.0	16	1.89	1 7/8	2.49	3 7/16	1 13/16	↓	↓
×233*	68.5	16.0	16	1.07	1 1/16	9/16	15.9	15 7/8	1.72	1 3/4	2.32	3	1 3/4	↓	↓
×211	62.0	15.7	15 3/4	0.980	1	1/2	15.8	15 3/4	1.56	1 9/16	2.16	2 7/8	1 11/16	↓	↓
×193	56.8	15.5	15 1/2	0.890	7/8	7/16	15.7	15 3/4	1.44	1 7/16	2.04	2 3/4	1 11/16	↓	↓
×176	51.8	15.2	15 1/4	0.830	13/16	7/16	15.7	15 5/8	1.31	1 5/16	1.91	2 5/8	1 9/8	↓	↓
×159	46.7	15.0	15	0.745	3/4	3/8	15.6	15 5/8	1.19	1 3/16	1.79	2 1/2	1 9/16	↓	↓
×145	42.7	14.8	14 3/4	0.680	11/16	3/8	15.5	15 1/2	1.09	1 1/16	1.69	2 3/8	1 9/16	↓	↓
W14×132	38.8	14.7	14 5/8	0.645	5/8	5/16	14.7	14 3/4	1.03	1	1.63	2 5/16	1 9/16	10	5 1/2
×120	35.3	14.5	14 1/2	0.590	9/16	5/16	14.7	14 5/8	0.940	15/16	1.54	2 1/4	1 1/2	↓	↓
×109	32.0	14.3	14 3/8	0.525	1/2	1/4	14.6	14 5/8	0.860	7/8	1.46	2 3/16	1 1/2	↓	↓
×99	29.1	14.2	14 1/8	0.485	1/2	1/4	14.6	14 5/8	0.780	3/4	1.38	2 1/16	1 7/16	↓	↓
×90	26.5	14.0	14	0.440	7/16	1/4	14.5	14 1/2	0.710	11/16	1.31	2	1 7/16	↓	↓
W14×82	24.0	14.3	14 1/4	0.510	1/2	1/4	10.1	10 1/8	0.855	7/8	1.45	1 11/16	1 1/16	10 7/8	5 1/2
×74	21.8	14.2	14 1/8	0.450	7/16	1/4	10.1	10 1/8	0.785	13/16	1.38	1 5/8	1 1/16	↓	↓
×68	20.0	14.0	14	0.415	7/16	1/4	10.0	10	0.720	3/4	1.31	1 9/16	1 1/16	↓	↓
×61	17.9	13.9	13 7/8	0.375	3/8	3/16	9.99	10	0.645	5/8	1.24	1 1/2	1	↓	↓
W14×53	15.6	13.9	13 7/8	0.370	3/8	3/16	8.06	8	0.660	11/16	1.25	1 1/2	1	10 7/8	5 1/2
×48	14.1	13.8	13 3/4	0.340	5/16	3/16	8.03	8	0.595	5/8	1.19	1 7/16	1	↓	↓
×43	12.6	13.7	13 5/8	0.305	5/16	3/16	8.00	8	0.530	1/2	1.12	1 3/8	1	↓	↓

*ASTM A6 tensile group 4 or 5 shape. Special requirements may apply per LRFD Specification Section A3.1c.
†See definition of "Workable Gage" in Nomenclature section at the back of this Manual.

Figure 2-2. Section properties of the W14×233 column [3].



(a) Base assembly.



(b) Header assembly.

Figure 2-3. Photograph of the column base and header assemblies prior to filling with concrete.



(a) Prior to modifications.



(b) After modifications.

Figure 2-4. Reaction wall at the MBTF site at EMRTC.



(a) Attachment of the rear reaction struts.

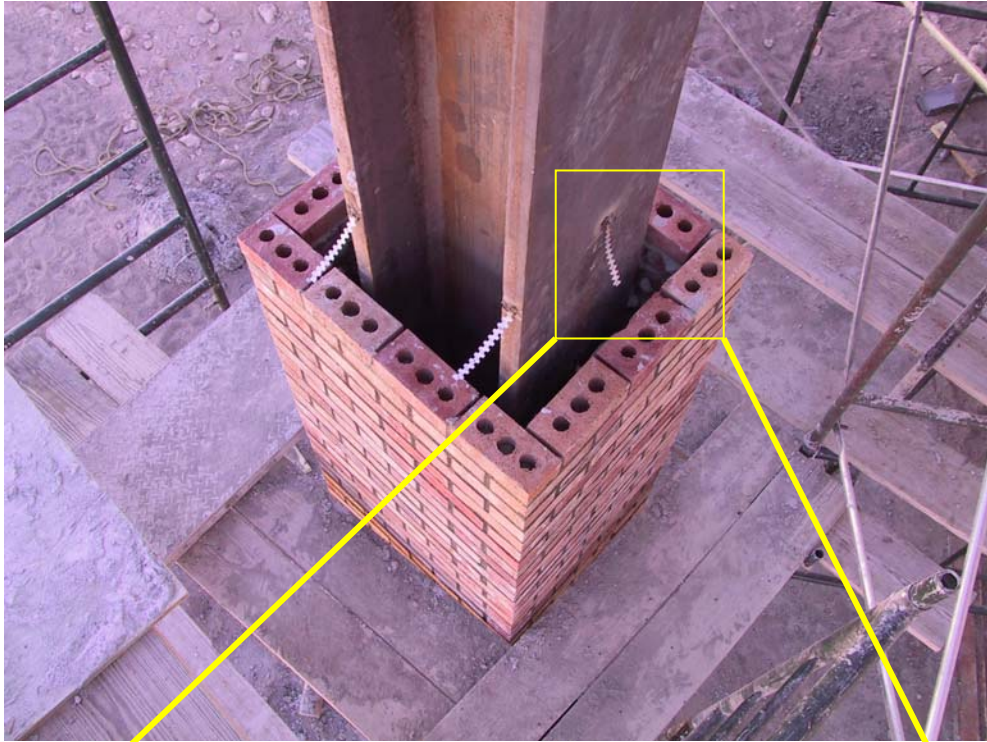


(b) Pouring of the base concrete.

Figure 2-5. Photographs of the installation of the test article to the MBTF reaction wall.



Figure 2-6. Photographs of the of the test article during curing of the footing.



(a) Corrugated wall ties used to provide lateral support to brick cladding.



(b) Close-up view of wall tie attachment to column.

Figure 2-7. Installation of the brick cladding enclosure around the test column.



(a) 2-6-2006



(b) 2-9-2006



(c) 2-10-2006



(d) 2-20-2006

Figure 2-8. Chronological view of AISC steel column cladding installation.

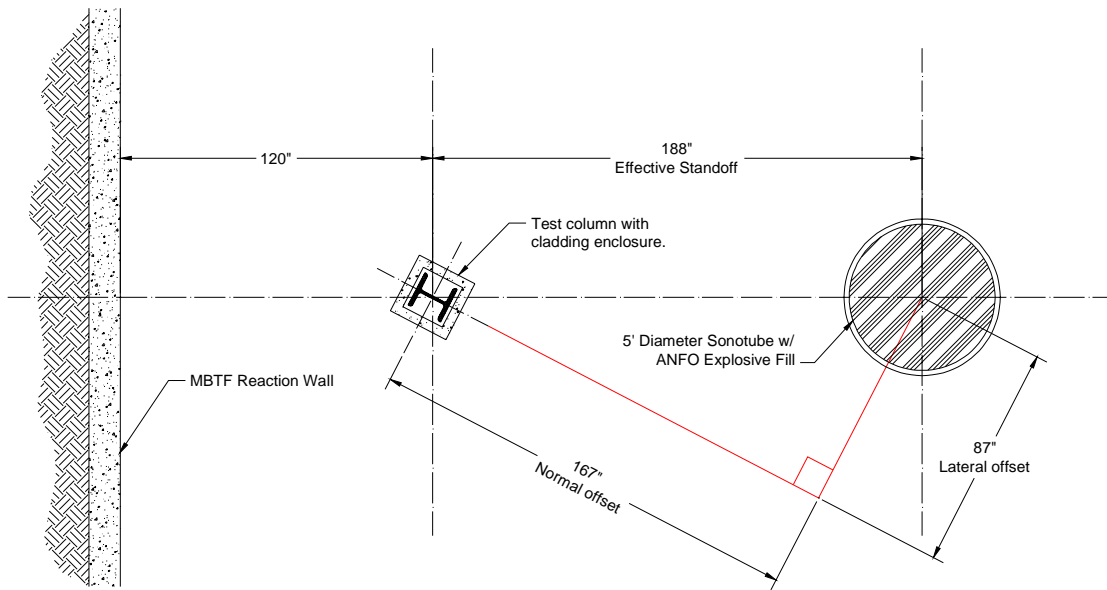


(a) View from grade.

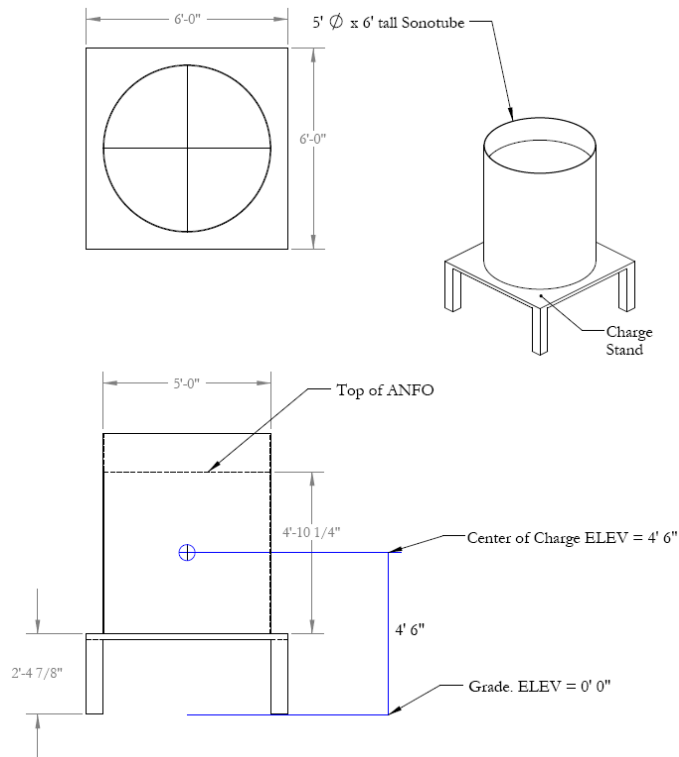


(b) View from top of reaction wall.

Figure 2-9. Photograph of the completed test column including the cladding enclosure.



(a) Charge standoff and layout.



(b) Charge stand showing the HOB.

Figure 2-10. Illustration of the positioning of the explosive to achieve an effective slant standoff of 15'-6" measured from the center of the column to the center of the charge. The normal offset was 167 inches (13.9 feet), the lateral offset was 87 inches (7.25 feet), and the height of burst (HOB) was 54 inches (4.5 feet).



(a) ANFO is filled halfway and the booster placed.



(b) ANFO is then completely filled and capped with plywood.

Figure 2-11. Photograph of a similar ANFO explosive setup using a Sonotube.



(a) South view of the test article.



(b) Northeast view of the test article.

Figure 2-12. Pretest photograph of the charge stand and explosive positioned at an effective slant standoff of 15'-6" measured from the center of the column to the center of the charge in the direction normal to the MBTF reaction wall.

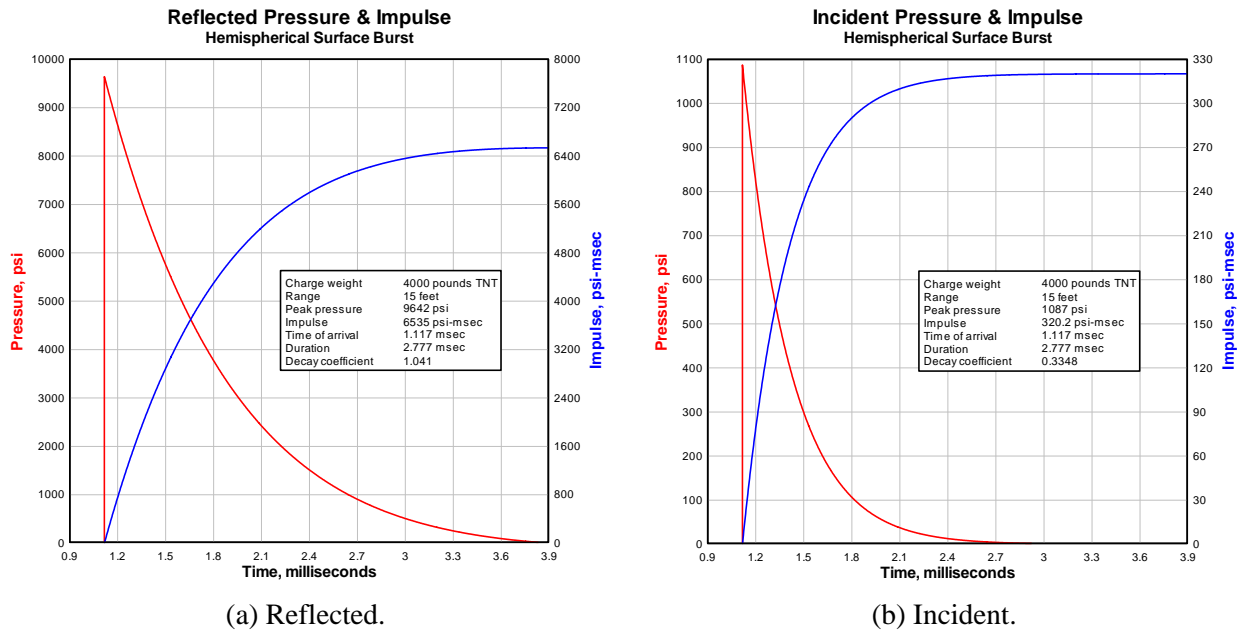


Figure 2-13. Estimate of the air blast loadings from 4,000 lb TNT at 15' standoffs for an ideal hemisphere on the ground surface.

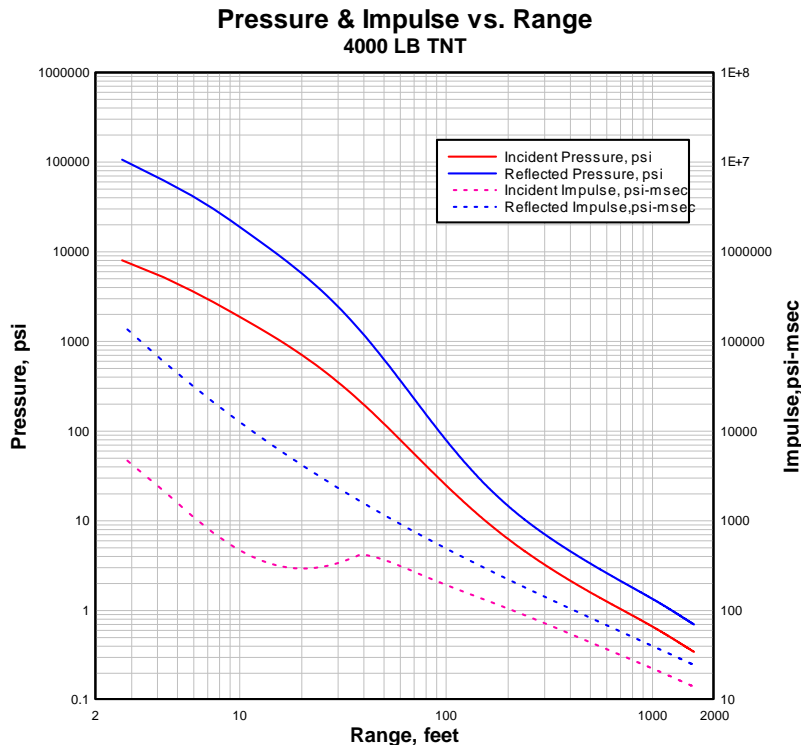
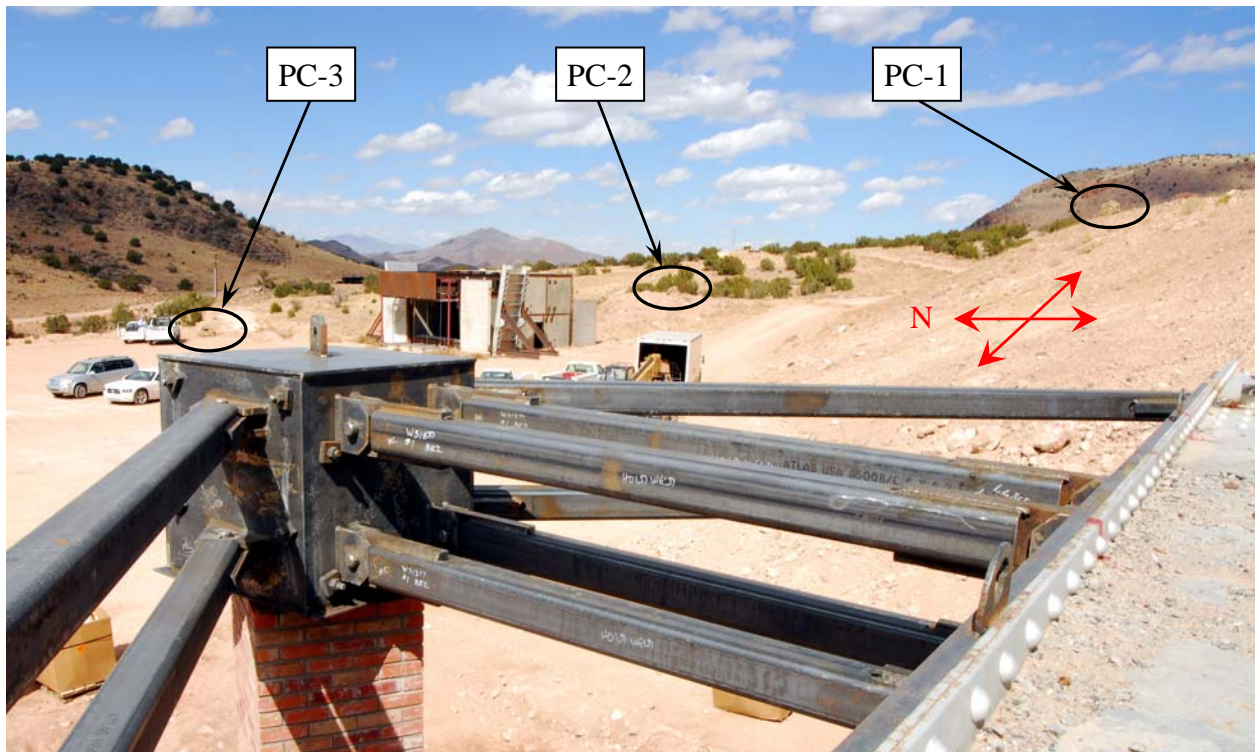


Figure 2-14. Air blast loadings versus range for an ideal 4,000-pound TNT hemisphere on the ground surface.



(a) Typical Phantom[®] high-speed digital camera w/ laptop computer shown installed in a protective steel box.



(b) Locations of the three Phantom[®] high-speed video cameras

Figure 2-15. High-speed video camera details.

This Page is Intentionally Left Blank

SECTION 3

TEST RESULTS

3.1 OBSERVED RESULTS

The test was executed on 2 March 2006 at 1430. Figure 3-1 shows a close-up view of the column taken from PC-1, taken moments after the detonation of the explosive. At 0.137 ms, the first light of the detonation process is visible in Figure 3-1a. Figure 3-1b, taken at 2.63 ms, shows the burning detonation products which have almost completely engulfed the column. The shockwave front has already impinged on the surface of the cladding at this time, although the interaction is obscured by the fireball. Unfortunately, this obscured view continues in the following sequences taken at 4.09 ms and 6.39 ms, as shown in Figure 3-1c and Figure 3-1d. These views, however, give a good visual of both the early time detonation process and the interaction of the test specimen with the detonation products.

Figure 3-2 shows a far-off view of the entire test bed taken from PC-3. Similar to the photographs taken by PC-1, the test bed is partially engulfed by the fireball at 4.19ms as shown in Figure 3-2a, and completely covered by 10.9 ms as shown in Figure 3-2b. The shockwave generated by the explosion is clearly visible from this same view at 14.2 and 30.9 ms in Figures 3-2c and 3-2d, which shows itself as a region of highly compressed air. The dust cloud visible in Figure 3-2d continues to expand and takes 10 to 20 seconds to clear the test bed.

The crater generated by the explosion is shown in Figure 3-3. The crater was essentially circular, having a diameter of roughly 108 inches and a depth of 14 inches. Generally it is difficult to measure the actual size of a detonation crater because significant amounts of loose ejecta typically fall back in place. It is thus likely that the actual crater was slightly larger than that indicated by the posttest measurements.

Figure 3-4 shows a pretest and posttest photograph of the column, viewing from the southwest direction (refer to Figure 2-12 for the test bed north key). The cladding was completely destroyed by the explosion—only small pieces of brick, between ¼” pieces of debris up to 3” fragments of the original brick, were the only remnants of the red brick cladding. Some of the largest pieces are visible in this figure. Even though the lateral struts show some permanent deformation, the reaction strut system and MBTF reaction wall successfully absorbed the large forces transmitted by the column, while imposing a fixed boundary condition to the test column component during the timeframe of its deformation.

As shown in Figure 3-5, the column sustained some permanent plastic deformation, but remained essentially intact. The majority of the column deformation occurred in the strong axis, in the southwest direction away from the explosion, localized around the base. This is clear from Figure 3-5a. The peak column deformation was 3.75 inches, occurring 42 inches above the footing. The column also sustained a small permanent deflection in the weak-axis direction, away from the explosive, on the order of 1 inch. This deformation was much more uniform and therefore indicative of flexural behavior, as seen in Figure 3-5b. There was no visible

deterioration of the concrete footing, indicating that the footing indeed provided a nearly rigid boundary restraint at the base.

Figure 3-6a and 3-6b show close-up views of the entire column from the southwest and southeast directions, respectively. The localized strong-axis deformation of the column is again clear in these photographs. It is also apparent from Figure 3-6a, that the eastern-most tip of the front flange sustained much more deflection than the column centerline where the flange meets the web of the section. On the other side as shown in Figure 3-6b, this same statement is also true for the western-most flange tip, although the effect is much less pronounced.

This localized deformation behavior at the base of the column is further illustrated in the series of photographs shown in Figure 3-7. The first six feet or so above the base of the column is shown in Figure 3-7a and 3-7b from west and east views, respectively. Isometric views of the forward flange, viewing southwest, and the rear flange, viewing northwest are shown in Figures 3-7c and 3-7d, respectively. These photos again reiterate the localized deformation near the base, with maximum deformations of between 24 to 48 inches above the base, and falling off with increasing height along the column. Also note again that the front flange tips were folded inward towards the interior of the section—an effect much more pronounced on the eastern-most flange tip. The rear flange tips, in contrast, deformed in a much more uniform pattern.

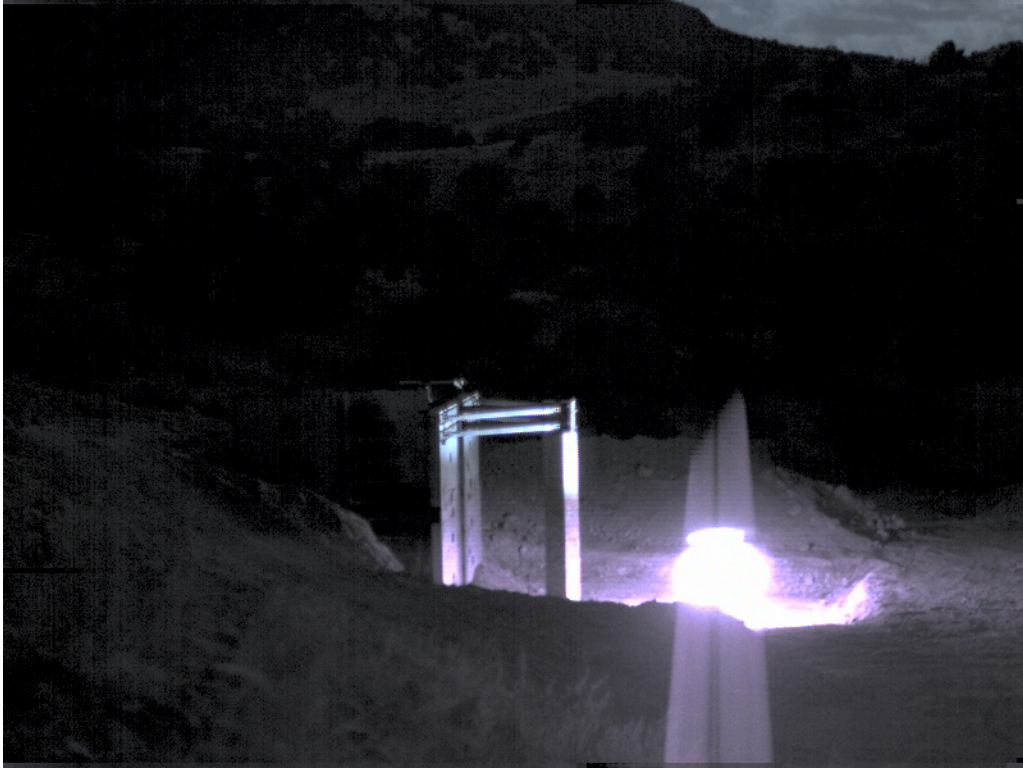
The response of the column is thus a combination of a shear and flexural response in the strong axis, and purely flexural in the weak-axis. The section did not appear to have significant torsional deformations. Furthermore, no fractures were observed in the section, including at the K-line region on the interior of the section that is known to have reduced ductility as a result of the steel milling process, nor at the front flange near the base which was clearly subjected to high strain-rate deformations.

3.2 COLUMN RESIDUAL DEFLECTION

In order to quantify the response of the column, a survey was performed to measure the residual plastic deformation of the column. As shown in Figure 3-8, a level was held adjacent to the base of the column, and the distance from the level to the column flange surface was measured and recorded. Such measurements were recorded to 54 inches of height above the base of the column. The deflections fell off quickly with increasing height above this point. The deflections of the flange centerline, which represents the deflection of the column web, as well as the deflections of the east-most and west-most flange edge tips are summarized in Table 3-1. These results are plotted as a function of height along the column in Figure 3-9. The peak web deformation was measured to be 3.75 inches, occurring at 42 inches above the base. The peak flange tip deformations were measured to be 6.38 inches and 4.50 inches for the north most and south most flange tips, respectively, both occurring 21 inches above the base. These results indicate that these flanges suffered net deflections, with respect to the web, of 2.63 inches and 0.75 inches, respectively.

Table 3-1. Residual deflection of the column as measured in a posttest survey. This table summarizes the residual deflection of the front column flange as a function of the column height.

Measurement	Height Along Column (in)	Residual Deflection		
		East Flange Edge (in)	Web Centerline (in)	West Flange Edge (in)
1	0.0	0.00	0.00	0.00
2	3.0	1.00	0.38	0.75
3	6.0	2.50	0.44	1.75
4	9.0	3.88	1.00	2.63
5	12.0	5.00	1.63	3.63
6	15.0	5.63	2.25	4.38
7	18.0	6.13	2.75	4.38
8	21.0	6.38	3.00	4.50
9	24.0	6.25	3.13	4.25
10	27.0	6.25	3.25	4.25
11	30.0	6.00	3.38	4.13
12	33.0	5.75	3.50	4.25
13	36.0	5.50	3.63	4.25
14	39.0	5.25	3.63	4.25
15	42.0	5.00	3.75	4.13
16	45.0	5.00	3.75	4.00
17	48.0	5.00	3.63	3.88
18	51.0	4.88	3.60	3.75
19	54.0	4.75	3.50	3.63
21	225.0	0.00	0.00	0.00



(a) $t = 0.137$ ms.



(b) $t = 2.63$ ms.

Figure 3-1. Close-up video stills of the test bed moments after detonation.



(c) $t = 4.09$ ms



(d) $t = 6.39$ ms

Figure 3-1. Close-up video stills of the test bed moments after detonation (Continued).

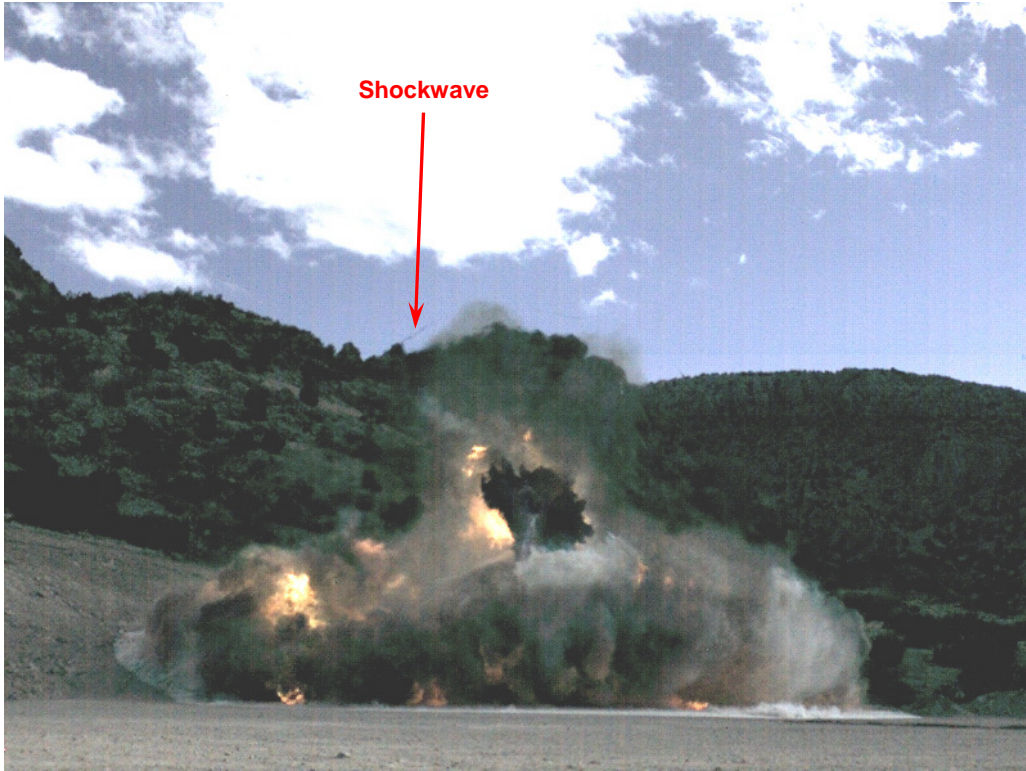


(a) $t = 4.19$ ms

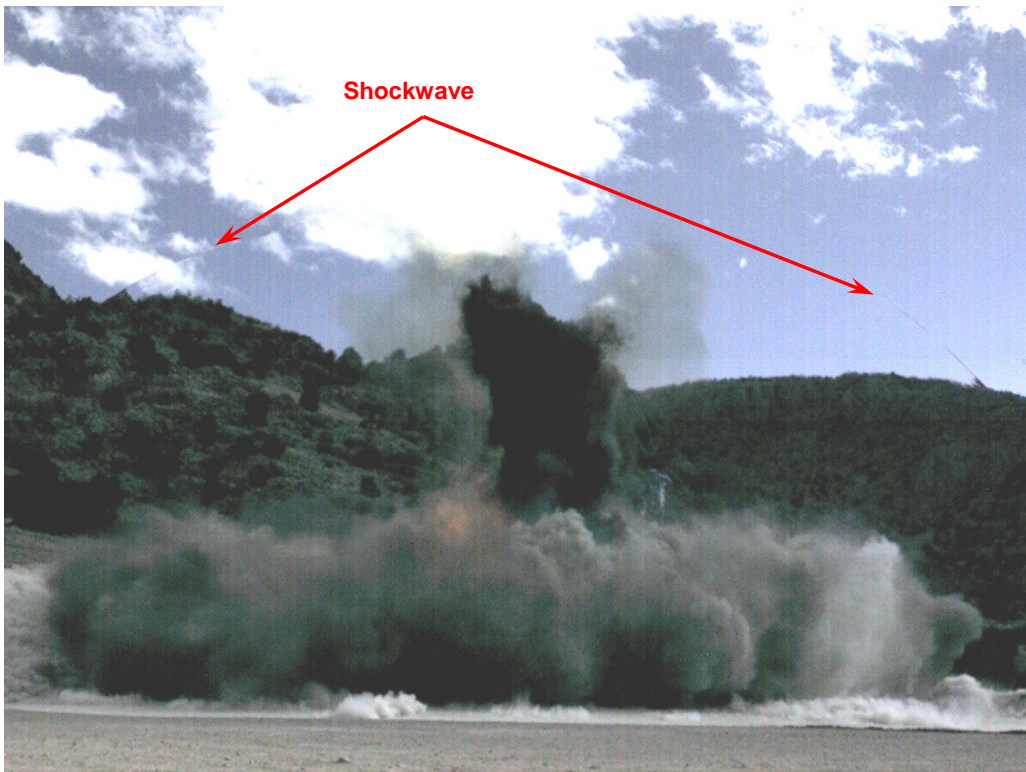


(b) $t = 10.9$ ms

Figure 3-2. Video stills of the test bed moments after detonation.



(c) $t = 14.2$ ms



(d) $t = 30.9$ ms

Figure 3-2. Video stills of the test bed moments after detonation (Continued).



(a) View of detonation crater diameter.



(b) View of detonation crater depth.

Figure 3-3. Posttest photograph of the detonation crater left by the explosion.



(a) Pretest.



(b) Posttest.

Figure 3-4. Pre and posttest photographs of the column.



(a) Viewing west.



(b) Viewing south.

Figure 3-5. Posttest photographs of the column and reaction system.



(a) Southwest view.

Figure 3-6. Close-up posttest photograph of the column.



(b) Southeast view.

Figure 3-6. Close-up posttest photograph of the column (Continued).



(a) West view.



(b) East view.



(c) Southwest view.



(d) Northwest view.

Figure 3-7. Posttest photographs of the base of the column.



(a) Viewing west.



(b) Viewing east.

Figure 3-8. Process of conducting the posttest survey of the column to quantify the residual deflection of the column's front flange as a function of height along the column.

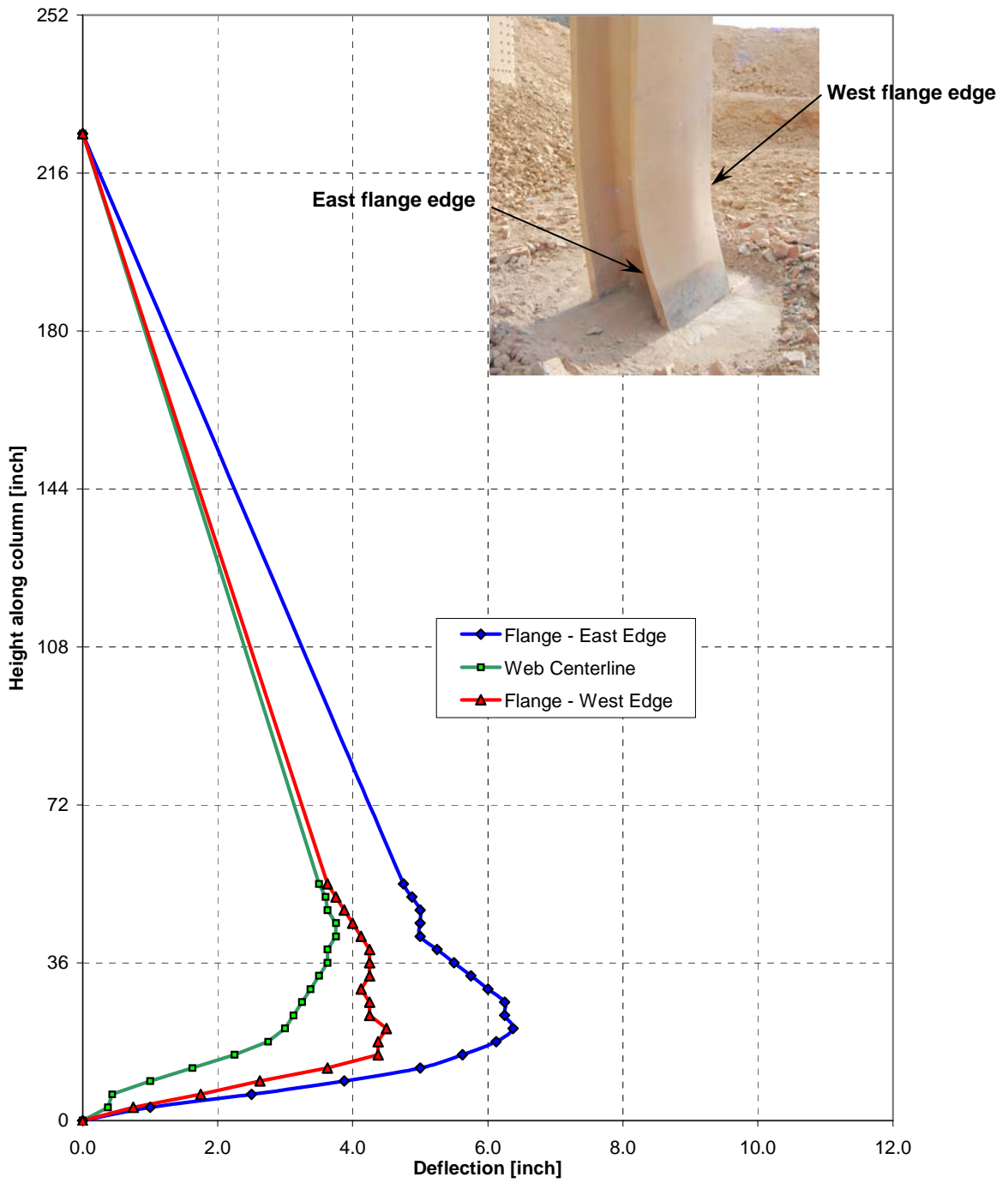


Figure 3-9. Residual deflection of the column's front flange as a function of height along the column.

This Page is Intentionally Left Blank

SECTION 4

DISCUSSION OF RESULTS

4.1 RESPONSE OF COLUMN

Although the column sustained permanent plastic deformation, the response of the column was in general well-behaved and the column likely retained its original axial load-carrying capacity. This is despite the rather complicated loading environment that the column experienced, which is illustrated in Figure 4-1.

Figure 4-1a shows a HFPB CFD computation of a similar large explosive directly across from a bare wide-flange column oriented in the weak-axis direction. This scenario is similar to the AISC column had the cladding been excluded from the test. As seen in the figure, a series of shock reflections occur on the interior of the section due to the shockwave impingement on the wide-flange section, creating loading on the interior of the section at both the web and the interior of the flanges. The resulting column response, as computed with HFPB CSD, is shown in Figure 4-1b, which shows severe local column deformations that essentially “open up” the section. This illustrates an important aspect of the behavior of wide-flange steel sections without cladding: sections will distort heavily in localized regions, though global deformation will be small. It is also important to note that localized fractures (i.e., fractures that result from stresses that exceed the ultimate shear and tensile strengths of the steel, not brittle cleavage fracture), have been observed experimentally for these cases because of this rather localized high strain-rate loading. However, this response is not particularly applicable to building structures, where there is almost always a cladding enclosure (as was the case in the AISC test) or an exterior cladding between the column and the explosive threat.

For these cases, the shock interaction with the column section is precluded, as cladding is typically massive enough to reflect the shockwave and shield the section from the initial shock front. Still, as illustrated in Figure 4-1c, the column is eventually loaded by the impact of the cladding with the column—an entirely different mechanism than the former. Consequently, the amount of loading can vary depending on the strength and fracture characteristics of the cladding material, any reinforcement placed in the cladding such as in RC precast panels, and the overall mass of the cladding material. For these reasons, columns having cladding have been observed, both experimentally and analytically, to sustain much more residual deflections at the global level, but much less residual deflection at the local section level. This is observed by comparing Figure 4-1c and 4-1b which were subjected to the same explosive charge and standoff.

Such was the case in the AISC column test, where the deformations are much more similar to those shown in Figure 4-1c. Still, as was described in Section 3, the column flanges did sustain localized “flange-folding” deformations, on the order of 1 to 3 inches more than the center of the flange. However, this is a result of the high-velocity cladding debris impacting the edges of the flanges, causing them to act essentially as cantilevered plates. Calculations performed by K&C for the FEMA/DHS effort [7], using simplified debris and conservative ConWep [4] loading models, yielded very similar results to those observed in the AISC test, indicating that the debris loaded the column rather than the shockwave impingement on the

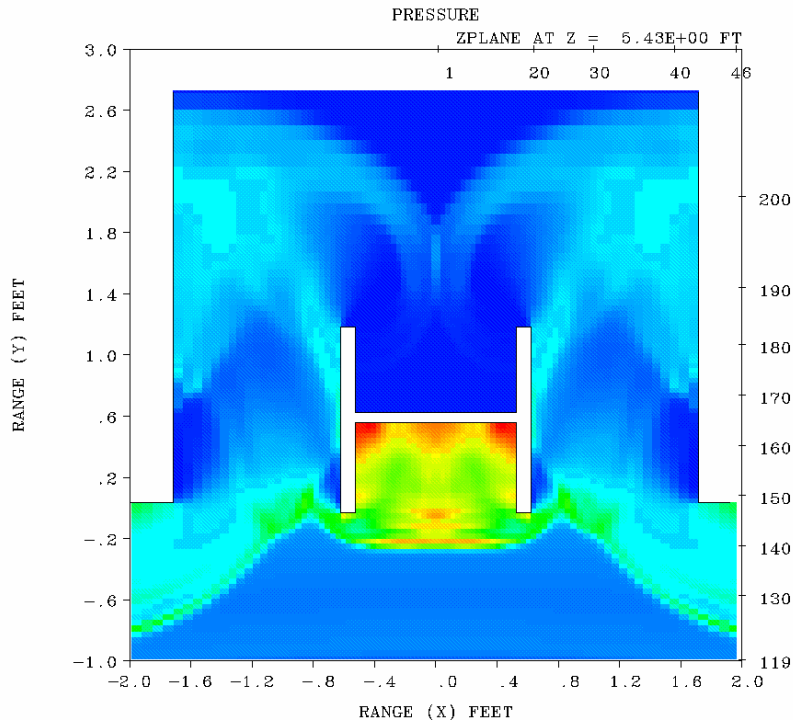
section. Results from those calculations are shown in Figure 4-2, for comparison with the posttest photographs of the AISC column which were shown in Section 3. Note the similarity in overall behavior captured in the computation. In that study, peak residual deflections were computed as 11 inches and 4 inches in the strong-axis and weak-axis, respectively, compared with 3.75 inches and 1 inch in the AISC test. This difference can be attributed to the various assumptions used in that simplified FE computation, including (1) conservative loads assuming a fully-reflected surface whereas the actual cladding provided a small finite surface (this greatly reduces the total impulse), (2) the idealization of the explosive as a hemispherical-shaped charge on the ground surface, while, as described earlier, the actual cylindrical shape and detonation mechanism will have significant effects on the pressure and impulse distribution at this close range, (3) assuming the debris was uniform and not connected prior to shockwave impingement (i.e., the computation does not account for the energy absorbed during the fracture of the cladding), and (4) modeling the interaction of the column with the pieces of debris as ideal elastic collisions. Nonetheless, despite these simplifications in the computation, whose purpose was to investigate the adequacy of the even more simplified calculations performed by ERDC using single-degree-of freedom (SDOF) structural response models and similar loading assumptions, the results compare reasonably well with the test.

For these reasons, SDOF calculations, such as those used by ERDC in the FEMA/DHS effort lend themselves well for providing an estimate of the column response for cases where cladding is present. Such models, based on ideal flexure behavior, assume that shear deformations are not dominant and that local fractures will not preclude flexural deformation of the structural member—assumptions that are quite valid in the case of the AISC column test specimen. The former assumption is discussed next within the context of the column test.

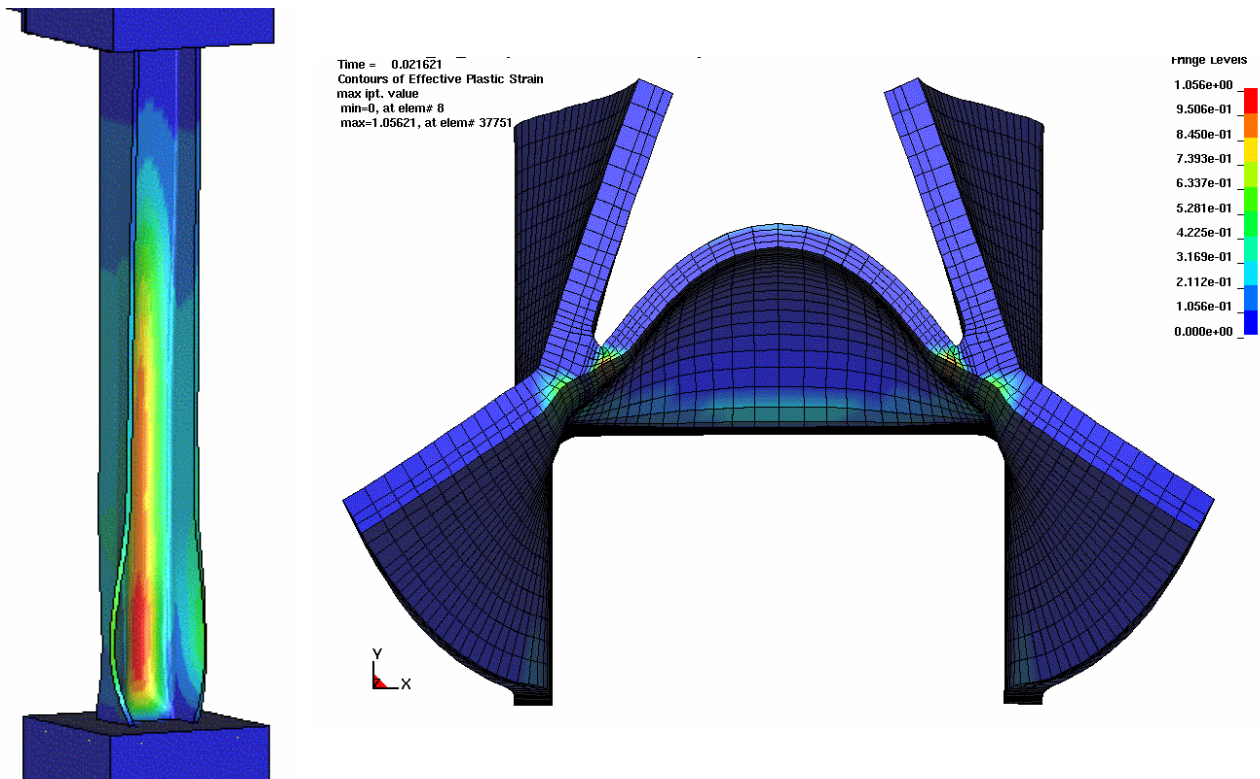
4.2 STEEL FRACTURE

Although some regions of the AISC column incurred high strain-rates and large local deformations, most notably near the base, areas of reduced ductility, such as the K-line region were not loaded with this same intensity. A separate set of tests on wide-flange sections subjected to small and close-in explosives [8, 9], showed a propensity for ductile fractures (i.e., fractures that result from stresses that exceed the ultimate shear and tensile strengths of the steel, not brittle cleavage fracture) to occur in the K-line region of the sections for worst-case loading orientations. Some of the failure modes observed in that limited test program are shown in Figure 4-3. Similar local failure modes are also being observed in a series of full-scale steel column tests subjected to large vehicle bombs funded by the Defense Threat Reduction Agency (DTRA) [10-15].

It is reassuring to note, however, that the only catastrophic local ductile fractures observed to date are in wide-flange sections without cladding. For these reasons, the AISC column test reiterates the robust and rather ductile behaviors that steel structures can exhibit for the majority of real terrorist threats. However, more testing is required to understand the regimes where local ductile fractures will occur, and to develop analytic models and simplified methods to help engineers design against these types of failures.

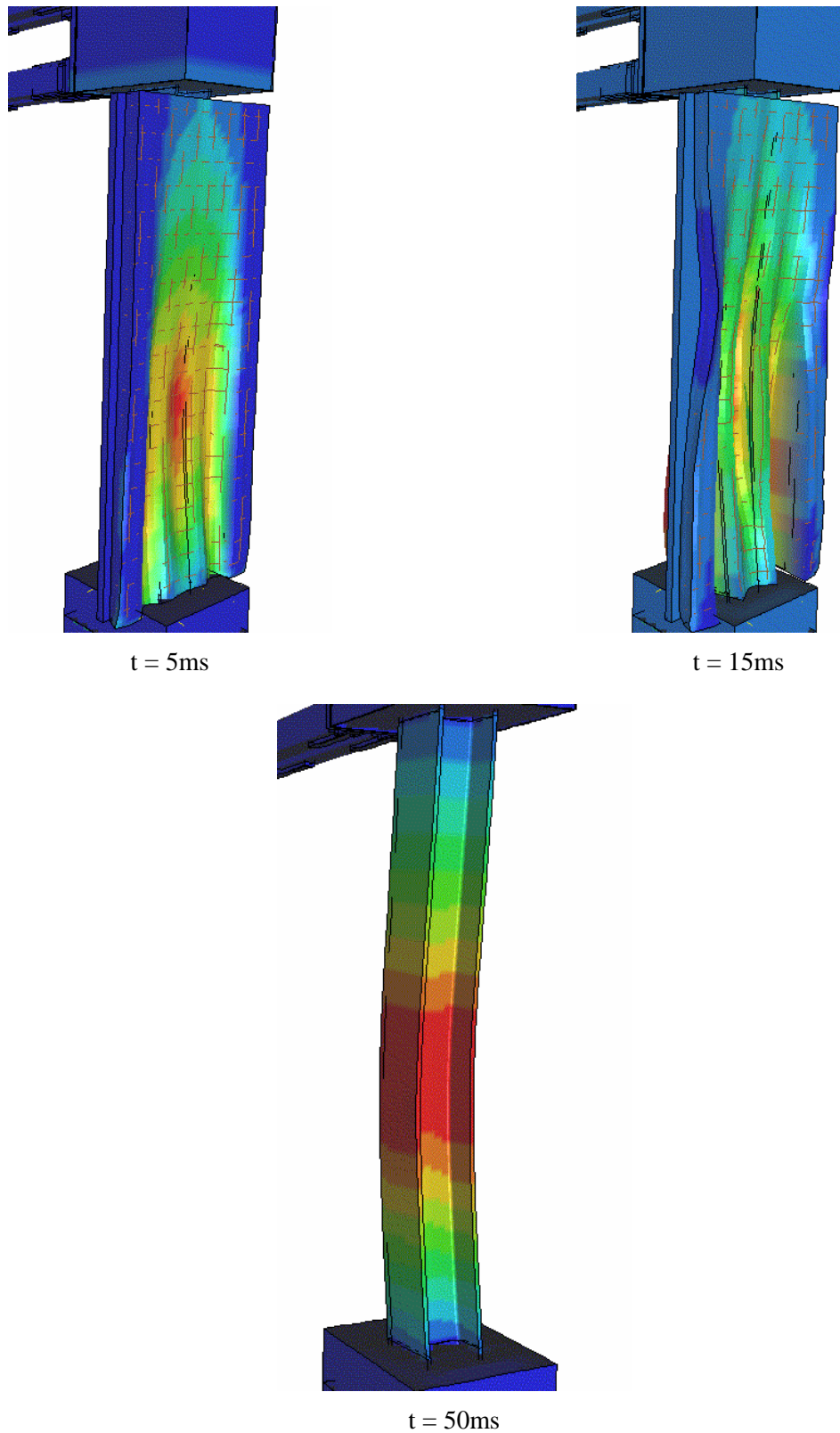


(a) Shockwave impingement on section without cladding, computed using HFPB CFD calculations.

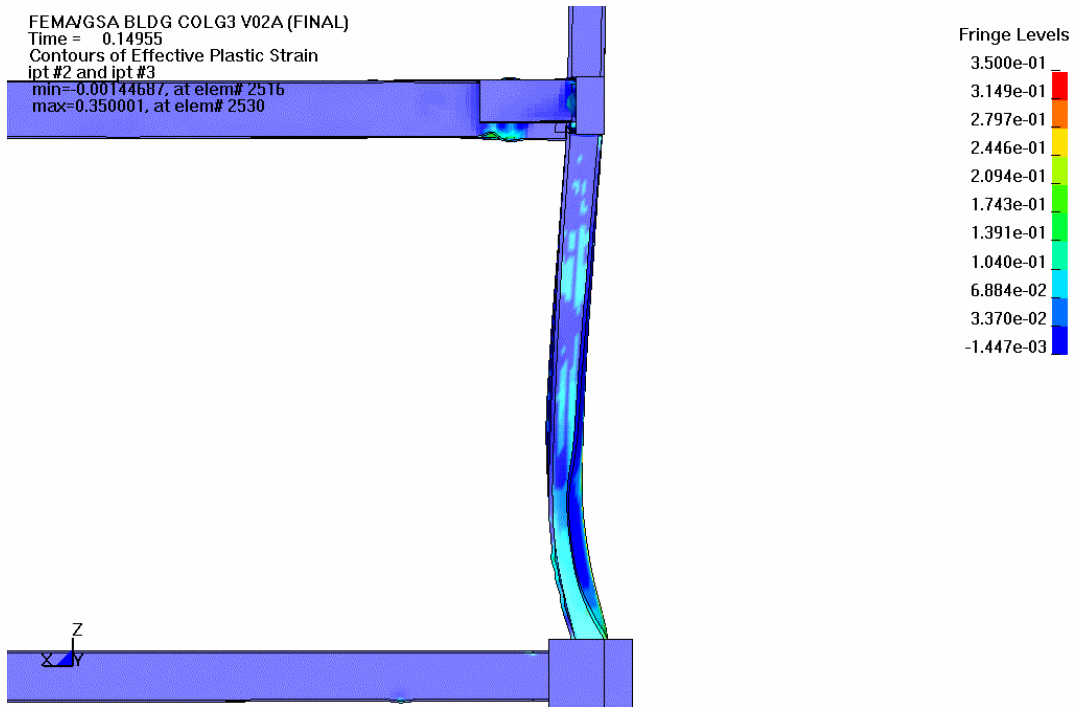


(b) Response of column without cladding, computed with HFPB CSD calculations.

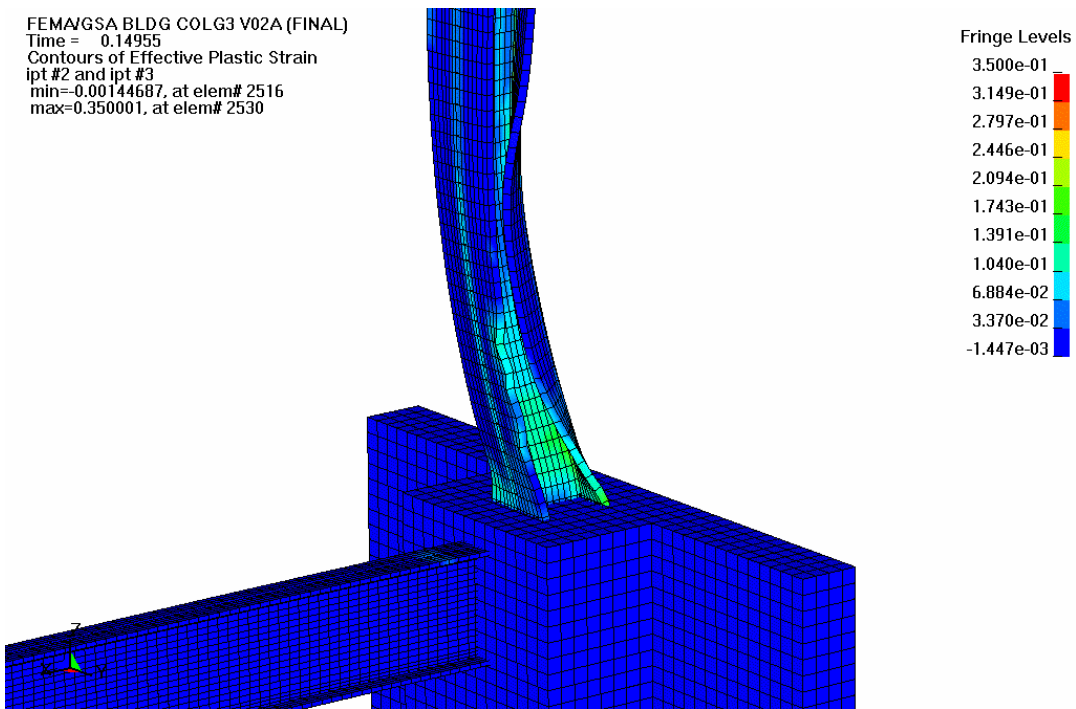
Figure 4-1. Variations in the response of steel wide-flange columns with and without cladding.



(c) Response of column with cladding, computed using HFPB CSD calculations.
Figure 4-1. Variations in the response of steel wide-flange columns with and without cladding (Continued).



(a) Side view of column deformation.



(b) Isometric view of base deformation.

Figure 4-2. Response of the 14WF228 column as computed using simplified HFPB FE calculations for the FEMA/GSA effort that include simplify loading methodologies [7].



(a) Ductile section response.



(b) Ductile fracture in K-line.

Figure 4-3. Failure modes of wide-flange sections as observed in a separate test program funded by AISC [8].

SECTION 5

CONCLUSIONS

5.1 CONCLUSIONS

The AISC column test was successfully executed on 2 March 2006, achieving the primary objective of experimentally determining the response of an 18'-9" tall W14×233 column subjected to a 4000-pound TNT-equivalent explosion at an effective slant range of 15'-6". The key conclusions from this test can be summarized as follows:

- The cladding was entirely destroyed by the blast effects. Small pieces of debris, on the order of ¼" up to 3" pieces of brick, were the only remnants of the red brick cladding used in the test.
- The column sustained a peak residual deflection of 3.75 inches in the strong-axis direction at 42 inches above the base of the column. Above this height, the deformations gradually fell back to zero with increasing height along the column. This strong-axis deformation mode of the column is best described as a combination of a shear and flexural response.
- A much smaller weak-axis deflection of roughly 1 inch occurred near midheight of the column. This deformation of the column in the weak-axis direction is best described as a purely flexural response.
- The front flanges of the column incurred localized deformations in the direction away from the explosive source which were much more dominant in the east-most flange tip (furthest from the explosion) than in the west-most flange tip. Specifically, the east-most flange tip deflected 2.63 inches more than the flange centerline, while the west-most flange tip deflected only 0.75 inches more than the flange centerline. The rear flange did not exhibit this behavior, and was clearly more uniform across the flange. This type of "flange-folding" behavior has been observed in other explosive tests on steel columns [10, 13, 15].
- No local fractures were observed in the column, indicating a significantly ductile behavior of the material, especially at the flange centerline near the base of the column which was clearly subjected to high strain-rates and large deformations.

5.2 RECOMMENDATIONS

Although the primary objectives of the test were successfully achieved, it is compelling to suggest recommendations for future research, especially when considering recent terrorist attacks on steel buildings and that research on structural steel response to blast effects is still in its infancy. These recommendations are aimed to provide data and design methodologies

directly to the construction and engineering design communities to best prevent collapse of structures from attacks on civilian structures using explosives. These include:

- Assessing the residual capacity of the AISC test column through loading the column to failure. Since the loss of a column in a structure can have a critical impact on the potential for progressive collapse of the structure, this data would help quantify the capacity of this column to sustain its original structural function despite being damaged by the explosion. Furthermore, load versus deflection curves for damaged structural elements are especially useful for structural engineers to analyze a structure for progressive collapse. Such data may also dispel certain progressive collapse provisions that require engineers to *assume* a steel column is lost from an explosion, and design an overly conservative building structure to span around the column, when the actual column may have significant residual capacity in a damaged state.
- Although portions of the test column incurred high strain-rates and large local deformations, the areas most prone to local ductile fractures (i.e., the K-line region) were not subjected to worst-case loadings during the AISC test. Furthermore, since ongoing test programs are indicating that structural steel is very robust in a blast environment, it is requisite that the regimes where these failures do occur be understood phenomenologically and analytically. Further tests similar to that conducted here will be extremely beneficial to this objective as well as compliment current ongoing efforts funded by the Department of Defense.
- Finally, only a special loading condition was tested here, where the column had a heavy cladding enclosure. For the majority of applications, and for a typical terrorist attack with a vehicle-bomb on the exterior of a building, analysis and available experimental data indicates that the type of cladding will affect the response of the column. For example, RC precast panels appear to impart much more loading into a column than one that exhibits no cladding at all. Since the projected area of the cladding tested in the AISC test did not have the capacity to fully reflect the shockwave, it would be beneficial to determine the response of the column, had the cladding been of another type of construction (e.g., precast panel, glass façade, etc.). This can readily be done analytically using HFPB CFD and CSD computations or experimentally with additional testing.

SECTION 6

REFERENCES

1. Hayes, J., R. Pekelnicky, S. Woodson, and C. Poland. "Blast-Resistance Benefits of Seismic Design Phase 1 Study: Performance Analysis of Reinforced Concrete Strengthening Systems Applied to the Murrah Federal Building Design". FEMA 439A. December 2005.
2. Historical Record Dimensions and Properties for Rolled Shapes-Steel and Wrought Iron Beams and Columns. American Institute of Steel Construction, Chicago, IL.
3. Manual of Steel Construction Load and Resistance Factor Design, 3rd Edition, American Institute of Steel Construction, Chicago, IL.
4. Hyde, D. W., "User's Guide for Microcomputer Programs ConWep and FunPro, Application of TM 5-855-1, 'Fundamentals of Protective Design for Conventional Weapons,'" Instruction Report SL-88-1, Department of the Army, Waterways Experiment Station, Corps of Engineers, Vicksburg, MS, March 2001.
5. "Structures to Resist the Effects of Accidental Explosions," Departments of the Army, the Navy, and the Air Force, Army TM 5-1300, Navy NAVFAC P-397, Air Force AFR 88-22, Washington, D.C., November 1991.
6. "Technical Manual Design and Analysis of Hardened Structures to Conventional Weapons Effects," The Departments of the Army, Air Force, and Navy and the Defense Special Weapons Agency, Army TM 5-855-1, Air Force AFPAM 32-1147(I), Navy NAVFAC P-1080, DSWA DAHSCWEMAN-97, August 1998.
7. Magallanes, J. M., and J. E. Crawford, "Analysis of a Steel Frame Subjected to Blast Effects and Subsequent Progressive Collapse Demands." Karagozian & Case, Burbank, CA, P-05-13. September 2005.
8. Crawford, J.E., and B. Dunn, "AISC Steel Materials Testing Final Report," Karagozian & Case, Burbank, CA, TR-05-1.1, January 2005.
9. Barson, J. M. and J. V. Pellegrino, "Failure Analysis of Steel Specimens Subjected to Blast Loads," AISC, January 2005.
10. Magallanes, J.M., K.B. Morrill, and J.W. Koenig, "Discrete Leto 7: Analytic and Test Results," Karagozian & Case, Burbank, CA, IR-05-49.1, September 2005.
11. Magallanes, J.M., K.B. Morrill, and J.W. Koenig, "Discrete Leto 8: Analytic and Test Results," Karagozian & Case, Burbank, CA, IR-05-59.1, February 2006.
12. Magallanes, J.M., J.W. Koenig, and P.J. Carpenter, "Discrete Leto 9: Analytic and Test Results," Karagozian & Case, Burbank, CA, IR-05-56.1, December 2005.

13. Magallanes, J.M., J.W. Koenig, and P.J. Carpenter, "Discrete Leto 10: Analytic and Test Results," Karagozian & Case, Burbank, CA, IR-06-05.1, January 2006.
14. Magallanes, J.M., J.W. Koenig, and P.J. Carpenter, "Discrete Leto 11: Analytic and Test Results," Karagozian & Case, Burbank, CA, IR-05-67.1, December 2005.
15. Magallanes, J.M., J.W. Koenig, and P.J. Carpenter, "Discrete Leto 12: Analytic and Test Results," Karagozian & Case, Burbank, CA, IR-06-13.1, February 2006.

APPENDIX A
TEST SPECIMEN CONSTRUCTION DOCUMENTS

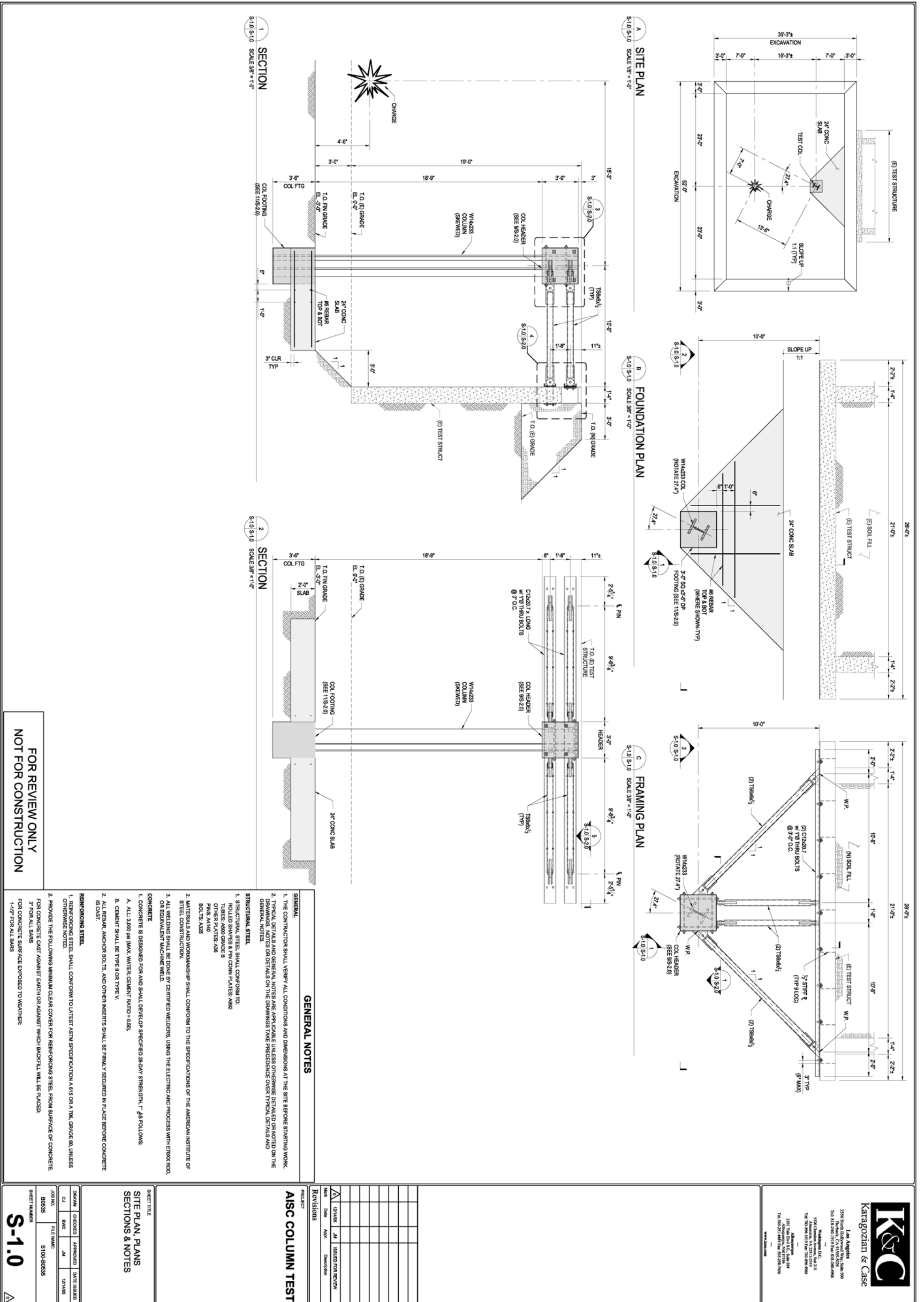


Figure A-2. K&C construction documents for AISC Column Test (1 of 2).

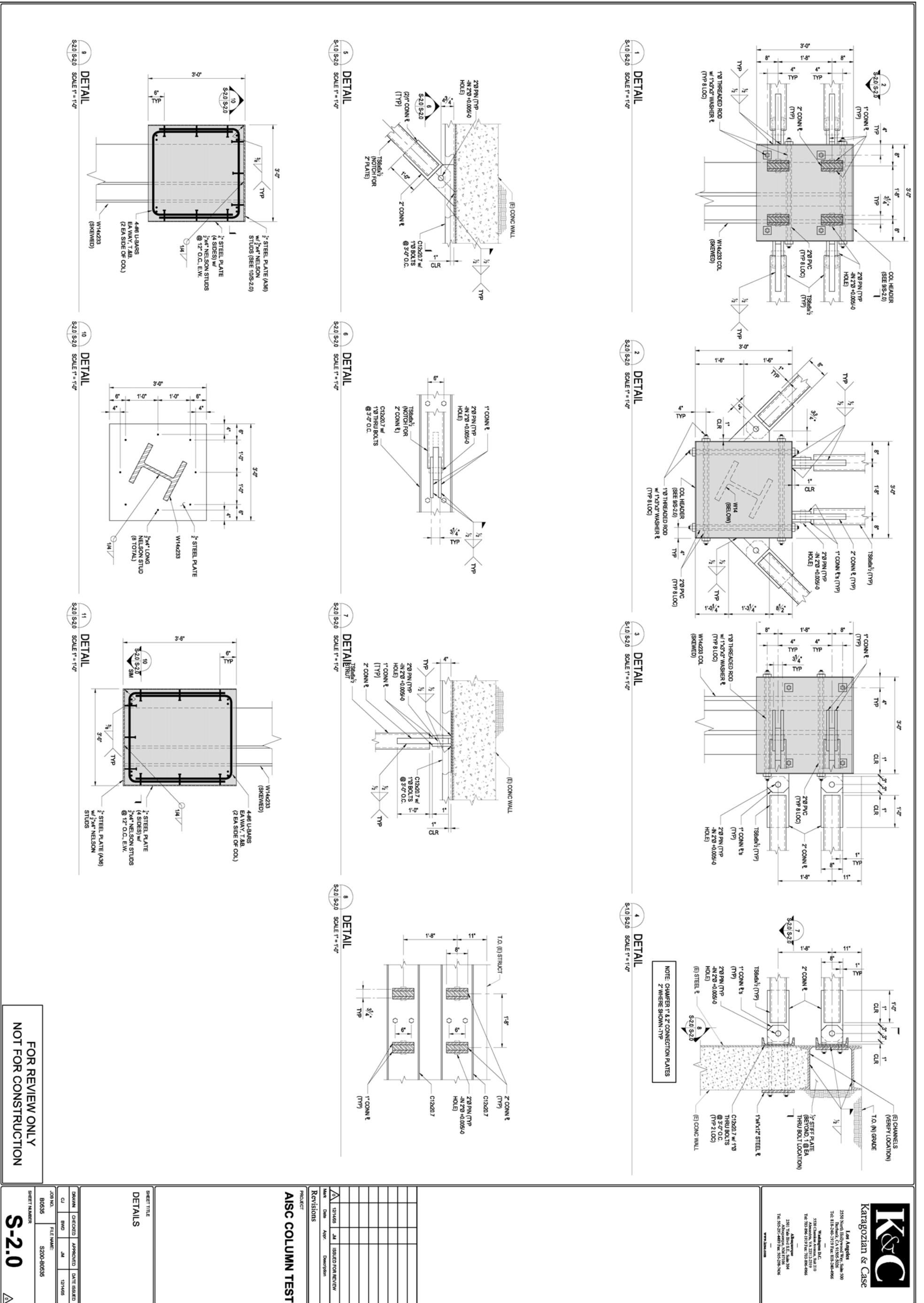


Figure A-3. K&C construction documents for AISC Column Test (2 of 2).

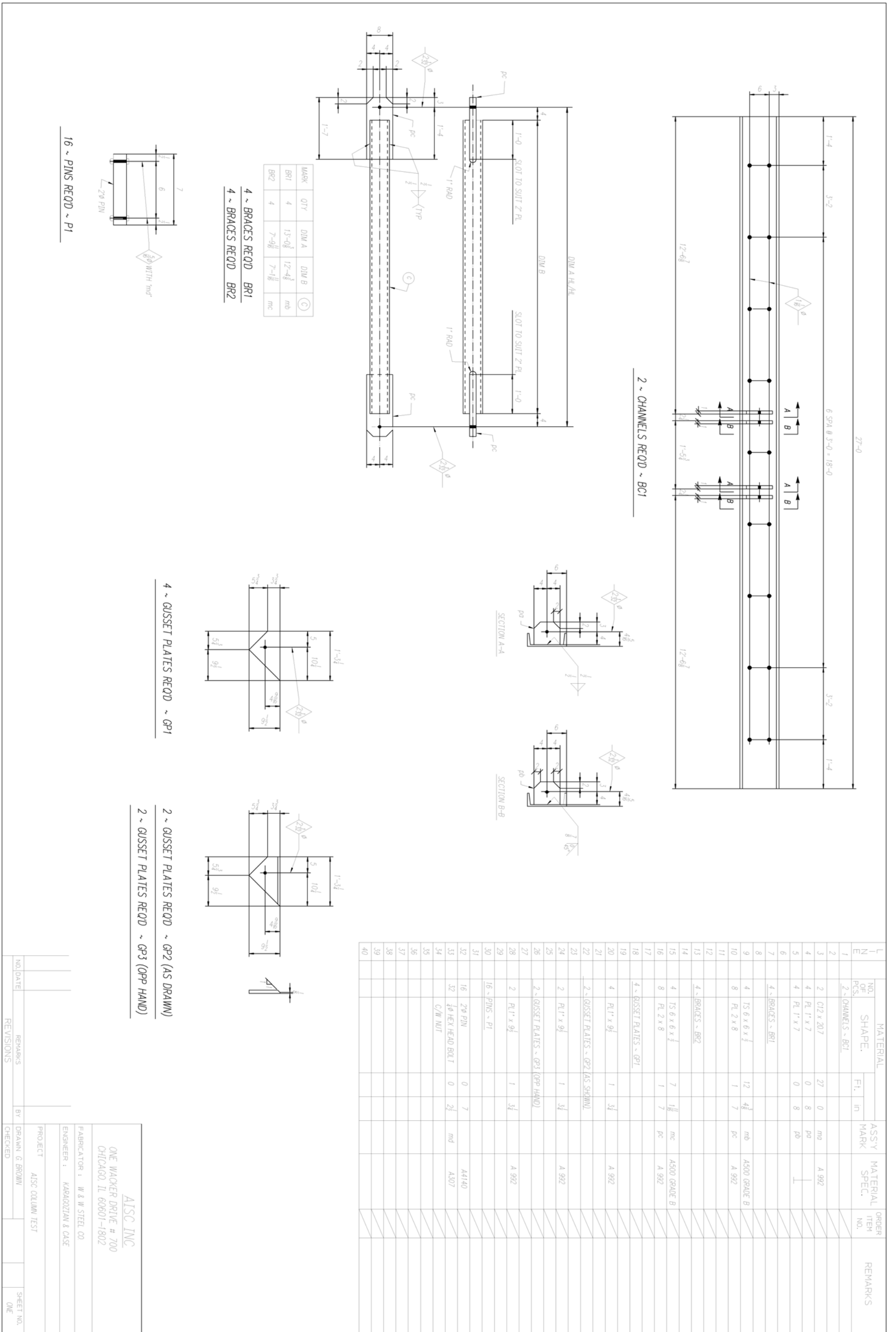


Figure A-4. AISC shop drawings for AISC Column Test (1 of 2).

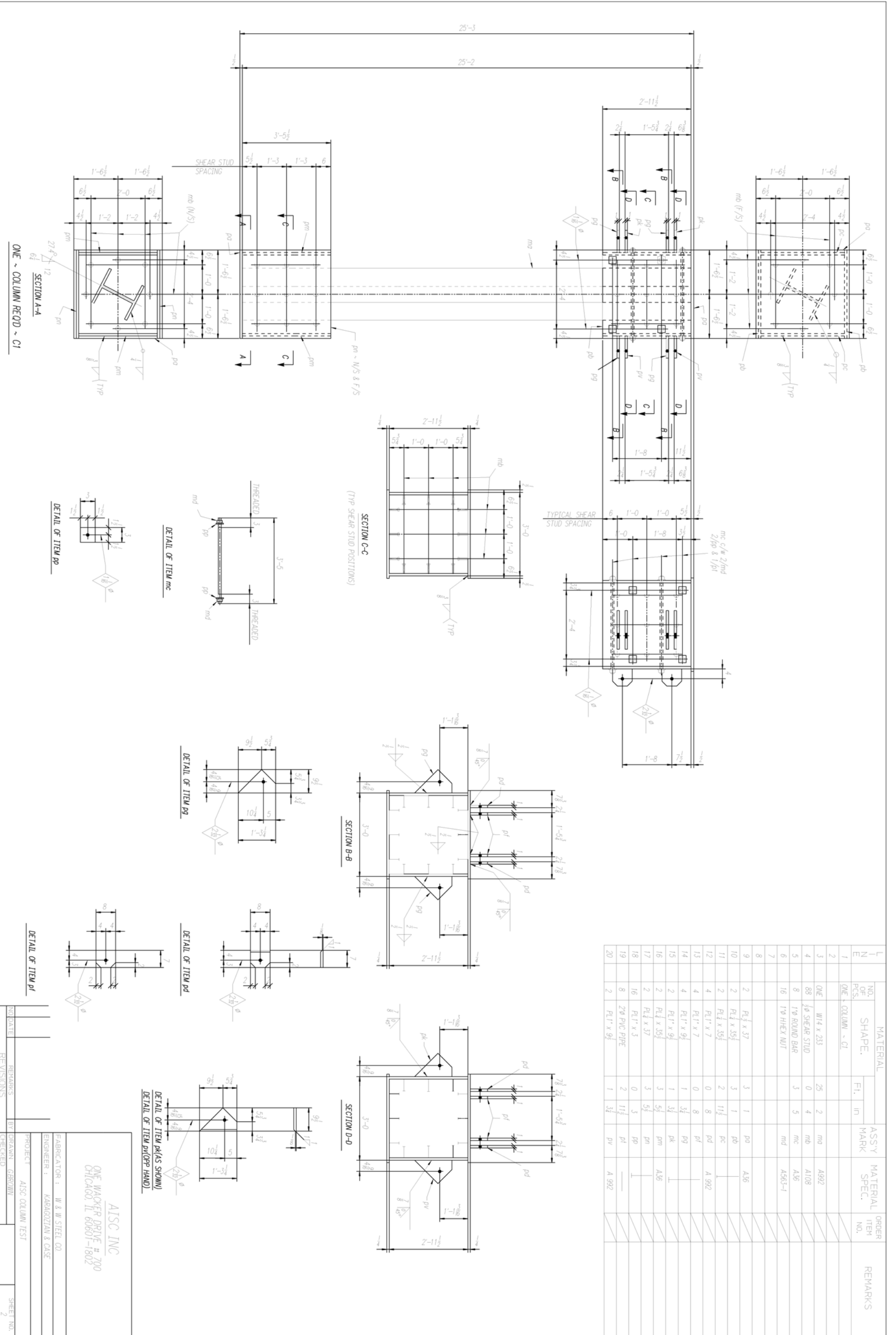


Figure A-5. AISC shop drawings for AISC Column Test (2 of 2).

Aboveground Airblast
 Hemispherical Surface Burst
 Charge weight 4878 pounds ANFO (AmNi/Fuel Oil)
 Equivalent weight of TNT 4000 pounds
 Range to target 15 feet

Peak incident overpressure..... 1087 psi
 Normally reflected pressure 9642 psi
 Time of arrival 1.117 msec
 Positive phase duration..... 2.777 msec
 Incident impulse 320.1 psi-msec
 Reflected impulse..... 6535 psi-msec
 Shock front velocity 8718 feet/sec
 Peak dynamic pressure..... 3271 psi
 Peak particle velocity 7512 feet/sec
 Shock density 0.537 lb/cubic foot
 Specific heat ratio..... 1.304 lb/cubic foot
 Decay coefficient α (msec), where
 $P(t)=P_{so}*[1-(t-t_a)/t_o]*\exp[-(t-t_a)/\alpha]$ 0.3348 lb/cubic foot

Figure A-5. ConWep output for 4,000 lb TNT charge at 15-foot standoff.